This is a preprint, the final version is subject to change, of the American Mineralogist (MSA)
Cite as Authors (Year) Title. American Mineralogist, in press.
(DOI will not work until issue is live.) DOI: http://dx.doi.org/10.2138/am-2017-5654

Revision 2

Trace elements and Sr-Nd isotopes of scheelite: Implications for the W-Cu-Mo polymetallic mineralization of the Shimensi deposit, South China

KEKE SUN[1] and BIN CHEN[2*]

[1]Key Laboratory of Orogenic Belts and Crustal Evolution, School of Earth and Space sciences, Peking University, Beijing 100871, China

[2]School of Resources and Environmental Engineering, Hefei University of Technology, Hefei 230009, Anhui, China

*Corresponding author: binchen@pku.edu.cn

This is a preprint, the final version is subject to change, of the American Mineralogist (MSA)
Cite as Authors (Year) Title. American Mineralogist, in press.
(DOI will not work until issue is live.) DOI: http://dx.doi.org/10.2138/am-2017-5654

ABSTRACT

The Shimensi deposit (South China) is a newly discovered W-Cu-Mo polymetallic deposit with a reserve of 0.76 million tones WO_3, one of the largest tungsten deposits in the world. We report elemental and Sr-Nd isotopic data for scheelites from the giant deposit, in order to determine the source region and genesis of the deposit. Scheelite is the most important ore mineral in the Shimensi deposit. Trace elements (including REEs) and Nd-Sr isotopic compositions of scheelites were used to constrain the origin of the mineralizing fluids and metals. Our data reveal that the REEs of scheelite are mainly controlled by the substitution mechanism $3Ca^{2+}=2REE^{3+}+\square Ca$, where $\square Ca$ is a Ca-site vacancy. Scheelites from the Shimensi deposit show negative Eu anomalies in some samples, but positive Eu anomalies in others in the chondrite-normalized REE patterns. The variation of Eu anomalies recorded the ore-forming processes. Considering the close spatial and temporal relationship between the mineralization and porphyritic granite, we think the negative Eu anomalies were inherited from the porphyritic granite and the positive ones from destruction of plagioclase of country rock during fluid-rock interaction. The variation of cathodeluminescence (CL) colour of a single scheelite from red to blue and to yellow was likely associated with the increase of REE contents. The scheelites hosted in the Mesozoic porphyritic granite with negative Eu anomalies formed in a primitive ore-forming fluid, whereas the scheelites hosted in Neoproterozoic granite with positive Eu anomalies precipitated in an evolved ore-forming fluid. The high Nb, Ta, LREE contents and LREE-enriched REE patterns of scheelites from the Shimensi

deposit reveal a close relationship with magmatic hydrothermal fluids.

The scheelites from the Shimensi deposit are characterized by low $\varepsilon_{Nd}(t)$ values (-6.1～-8.1) and unusually high and varied initial $^{87}Sr/^{86}Sr$ ratios (0.7230～0.7657). The $\varepsilon_{Nd}(t)$ values of scheelites are consistent with those of the Mesozoic porphyritic granite, but the Sr isotopic ratios are significantly higher than those of the granites, and importantly, beyond the Sr isotopic range of normal granites. This suggests that the ore-forming fluids and metals cannot be attributed to the Mesozoic porphyritic granites alone, the local Neoproterozoic Shuangqiaoshan Group schists/gneisses with high Rb/Sr ratios and thus radiogenic Sr isotopic compositions should have contributed to the ore-forming fluids and metals, particularly, in a later stage of ore-forming process, by intense fluid-rock interaction. This is different from a commonly accepted model that the ore-forming fluids and metals were exsolved exclusively from the granite plutons.

Keywords: Scheelite; trace element; REE; Sr-Nd isotopes; Shimensi

INTRODUCTION

Scheelite is one of the two tungsten ore minerals, being exploited mainly in skarn deposits, and effectively, is an important ore mineral in many other ore deposits such as porphyry-type, quartz vein-type and some metamorphic type deposits (Allen and Folinsbee 1944; Xu 1957; Noble et al. 1984; Liu and Ma 1987; Zhang et al. 1990; Uspensky et al. 1998; Peng et al. 2003; Wang et al. 2008; Song et al. 2014). Scheelite has a simple crystal structure with tetrahedral $[WO_4]^{2-}$ groups and irregular

dodecahedral $[CaO_8]^{14-}$ groups, and can accommodate high concentrations of rare earth elements (REEs), Y, Sr and Pb in substitution for Ca (Cottrant 1981). It is of particular interest to ore geologists because it has the potential to provide important information on the genesis of ore minerals and related deposits (Zhang et al. 1990; Brugger et al. 2008). The REE abundances of scheelite can be used to infer the origin of ore-forming fluids, source characteristics and mineralization conditions (Tomschi et al. 1986; Brugger et al. 2008). Scheelite is one of the few minerals characterized by high Sm/Nd ratios and is therefore potentially useful for Sm/Nd dating and Nd isotopic study (Kempe et al. 2001; Peng et al. 2003; Roberts et al. 2006). In addition, the scheelite lattice can accommodate small amounts of Sr but reject Rb (Deer et al. 1966) and thus the radiogenic ^{87}Sr from ^{87}Rb decay has a negligible effect on Sr isotope compositions of scheelite (Bell et al. 1989). The Sr and Nd isotopic compositions of scheelite have been extensively used to constrain the origin of the mineralizing fluids and solutes in Archaean gold deposits (e.g., Mueller et al. 1991; Kent et al. 1995; Darbyshire et al. 1996; Frei et al. 1998), and the evolution of W mineralization in complex tectonic settings (Eichhorn et al. 1997).

A cluster of W-rich districts, including the Dahutang W-Cu-Mo, Xianglushan W, Yangchuling W-Mo, and Zhuxi W-Cu-Mo deposits, have been discovered on the northern margin of the Jiangnan Orogen in the South China craton in recent years (Mao et al. 2013). The Dahutang ore field consists of three ore deposits: the Shimensi deposit in the north, Dalingshang deposit in the center and the Shiweidong deposit in the south, containing estimated reserves of 2 million tons of WO_3, 500 Kt Cu and 80.2

Kt Mo with average grade of 0.152% W, 0.12% Cu and 0.098% Mo, respectively. Scheelite is the most important ore mineral in the Shimensi deposit. Extensive studies focused on scheelite of hydrothermal gold deposits, but few on tungsten deposits in recent years. The Shimensi deposit offers the opportunity to use detailed geochemistry of the scheelite to get information on the genesis of a non-skarn large scheelite deposit. In this paper, we use the in-situ major and trace elements, cathodoluminescence (CL) images and Sr-Nd isotopes of scheelites from the Shimensi deposit, with the purpose to place constrains on (1) the origin, nature and evolution of ore-forming fluids, and (2) the origin of ore-forming metals, especially tungsten.

GEOLOGICAL SETTING

The South China Craton is composed of the Yangtze Block in the northwest and Cathaysia Block in the southeast. The ca. 1500km long ENE-trending Neoproterozoic Jiangnan Orogen occurs in the southeastern margin of the Yangtze block (Fig. 1; Huang and Jiang 2014), and is considered to have resulted from collision of the Yangtze and Cathaysia blocks at the end of the formation of the Rodinia supercontinent (e.g., Charvet 2013; Yao et al. 2013). On a geophysical basis, the Jiangshan-Shaoxing fault (the southern boundary of the Jiangnan orogen), is usually taken as the Yangtze-Cathaysia block boundary (Wang et al. 2013), and the Jiangnan orogenic belt (thrusted terranes onto the Yangtze block) is therefore considered as part of the Yangtze block.

The Jiangnan Orogenic belt is an accretionary orogeny, involving Neoproterozoic

arc terranes, affected by a low grade (greenschist facies) metamorphism and syn-schistose deformation, and ending with the intrusion of the undeformed Neoproterozoic granites, known as the Jiuling granite (ca. 819 Ma) (Li et al. 2003； Zheng et al. 2007). Following the end of the Jiangnan orogeny, all these terranes were eroded and unconformably covered by a rift sequence, called the Nanhua rift sequence, deposited in a series of aborted rifts of Cryogenian age (ca. 820-ca. 750Ma) (Wang and Li 2003； Wang et al. 2014,), and followed by terrigenous sedimentation from the Ediacaran (Sinian) to the Middle Ordovician (Charvet et al. 2010). During the Jurassic and the Cretaceous, a giant granitic province was formed in the South China craton, responding to the intense Mesozoic Yanshanian events, with two major peaks of granite emplacement, the Early Yanshanian event (ca. 180-140 Ma) and the Late Yanshanian event (140-97 Ma) (Zhou and Li 2000). Most of the granites and associated deposits are located in the Cathaysia block, but the Yanshanian granite province overlapped the Yangtze-Cathaysia boundary, and the Shimensi deposit of this study is genetically associated with the Late Yanshannian granite plutons as described below.

< Fig. 1 >

GEOLOGY OF THE SHIMENSI DEPOSIT

Structures and ore-related granites

The Shimensi W-Cu-Mo deposit, and many other polymetallic deposits as well (Mao et al. 2013), is confined to the Jiangnan orogen that is made up mainly of the Neoproterozoic Jiuling granites and the Shuangqiaoshan group greenschist facies

meta-sedimentary rocks including turbiditic rocks, pelite, tuffaceous sandstone, phyllite, tuff, phyllitic slate and less spilite and quartz-ketatophyre (BGMRJX 1984; Shu and Charvet 1996; Liu 1997). A series of EW-striking shear zones (ca. 100m width) occur in the Neoproterozoic granite, which are highly silicified, and intersected by the 25km long NNE-trending Xianguoshan-Dahutang-Shiweidong basement fault in the north of the Shimensi deposit. These two sets of faults are considered to have been the channels of the ore-forming fluids, and they not only controlled the distribution of the deposits, but also determined the emplacement of the Mesozoic granites in study area (Fig. 2a). In addition, several NNE-NE and NNW-NW trending, NW and NE dipping faults of variable length between 100 m and 500 m, can be observed in the deposit.

< Fig. 2 >

Major granites associated with the W-Cu-Mo mineralization in the Shimensi deposit are the Mesozoic porphyritic granite, fine-grained granite and granite porphyry, which occurred as stocks intruding into the Neoproterozoic granite (Fig. 2b). The porphyritic granite is the dominant rock type, with zircon U-Pb ages of around 147±1 Ma (Mao et al. 2014). This granite contains 30% quartz, 40~45% K-feldspar, 5~10% plagioclase, 10% biotite and 5~10% muscovite, and accessory apatite, zircon, fluorite and ilmenite, with medium- to coarse-grained phenocrysts of plagioclase, K-feldspar, quartz and biotite and minor muscovite. Scheelite coexists with wolframite occurring in plagioclase.

The fine-grained granite intruded into the porphyritic granite, and locally into the

Neoproterozoic granite (Fig. 2b and 2c), with zircons ages of 144.7±0.5 Ma~146.1± 0.6 Ma (Mao et al. 2014). It is composed of 30% quartz, 45% K-feldspar, 10% plagioclase, 10% biotite and 5~10% muscovite, and accessory zircon, fluorite, apatite and ilmenite. Compared with the porphyritic granite, the fine-grained granite contains more groundmass. Scheelite and some sulfide minerals like pyrite and pyrrhotite are associated with sericitization in the fine-grained granite.

The granite porphyry dikes (with variable width of 20 cm to 80 cm) are scattered throughout the Shimensi deposit. They intrude into both the porphyritic granite and the fine-grained granite (Figs. 2b and 2c), with emplacement ages of 143.0±0.76 Ma~143.1±1.2 Ma (Mao et al. 2014). The granite porphyry is composed of 40% quartz, 40% K-feldspar, 5~10% plagioclase, 5% biotite and 5~10% muscovite, and accessory zircon, apatite, and fluorite, with phenocrysts of K-feldspar, quartz and biotite, and groundmass of K-feldspar, quartz, fluorite and muscovite. Pyrite and chalcopyrite mineralization can be found in the granite porphyry.

Feng et al. (2012) reported a molybdenite Re/Os age of 143.7±1.2 Ma for the Shimensi deposit, which is consistent with the emplacement ages of the three types of granites. Nevertheless, based on the spatial relation between the tungsten mineralization and the porphyritic granite, we think the tungsten mineralization was mainly associated with the porphyritic granite, but tungsten mineralization can be seen in other two rock types as shown in Fig 2b. Overall, the W-Cu mineralization is subordinate in the Mesozoic granites, but confined mostly to the Neoproterozoic granite near the contacts with the Mesozoic porphyritic granite as shown in Fig 2c.

The ore bodies usually are layered to lenticular with a maximum thickness of ~390 m. Detailed descriptions for the mineralization features are as below.

Mineralization characteristics

Three mineralization types are observed in the Shimensi deposit, which are (1) veinlets-type mineralization, (2) breccia-type mineralization, and (3) quartz vein-type mineralization. Type 1 mineralization is the dominant ore type, with >90% of the total tungsten reserves. The ore-bearing quartz veinlets commonly have width of 0.5 - 2 centimeters (Figs. 3a and 3b), which were densely distributed in the Neoproterozoic granite and sparsely in the Mesozoic porphyritic granite (Fig. 2c). The major ore mineral is scheelite, accompanied by small amounts of wolframite, cassiterite, and chalcopyrite. Scheelite occurs as fine-grained and anhedral grains, being crosscut by chalcopyrite (and molybdenite, not shown; Fig. 3c). The gangue minerals are quartz, biotite, muscovite, and fluorite. The mineralization is closely related to greisenization, and the muscovites contain muscovite (62%~79%), celadonite (4%~15%), ferroceladonite (7%~22%) and paragonite (4%~11%) (Table 1.1).

< Fig. 3>

Type 2 breccia-type mineralization, containing ca. 5% of the total WO_3 reserve in the ore field, was situated mainly in the apical part of the Mesozoic porphyritic granite (Fig. 2b). The breccia fragments consist mainly of the Neoproterozoic granite and subordinate Mesozoic porphyritic granite (Fig. 3d), which show internal jigsaw textures welded by ore-bearing quartz. The ore minerals are early-stage scheelite and wolframite, and late-stage chalcopyrite and molybdenite (Fig. 3e). Molybenite and

chalcopyrite could have precipitated simultaneously from the ore-forming fluids, because they show intergrowth relationships (Fig. 3f; Wang et al. 2015). Gangue minerals include quartz, muscovite, K-feldspar, biotite and fluorite.

Type 3 quartz vein-type mineralization accounts for ca. 1% of the total ore reserve with a high tungsten grade (average of 0.282% WO_3) (Fig. 2b). The ore-bearing quartz veins commonly have widths of 10-50 centimeters, with ore minerals of wolframite, chalcopyrite and scheelite. Wolframite usually occurs as thick tabular crystals, rooted in the vein walls, forming a com-like structure (Fig. 4a). Wolframite was replaced partially by chalcopyrite, which subsequently cut by scheelite, suggesting a formation order from earlier wolframite to chalcopyrite and scheelite (Figs. 4b and 4c). This mineralization type cross-cuts all the granites and the other two ore types, indicative of the latest mineralization in the Shimensi deposit. Microprobe analysis of wolframite indicates that it has more ferberite than huebnerite with FeO = 9.28%~18.70% and MnO = 6.43%~15.11% (Table 1.2). Data of fluid inclusions hosted in scheelite and quartz indicate that the ore-forming fluids are characterized by low salinity (1%~9% NaCl; unpublished data) and low fO_2 as suggested by the presence of CH_4 in the inclusions (Fig. 4d).

< Fig. 4 >

The ore-forming process can be described as below, based on our new field investigation and petrographic observations. First, the Mesozoic porphyritic granite was intruded into the Neoproterozoic granite and pegmatite shells were formed at the contacts between the two rock units (Fig. 2c). The pegmatite shells consist of

K-feldspar, quartz, and small amounts of biotite and muscovite (Fig. 4e), which are commonly associated with W-Sn granites, such as those of the central European Erzgebirge (Altenberg) (Rösler et al. 1968). Potassic alteration was widely developed in this stage, converting plagioclase in the Neoproterozoic granite into K-feldspar (Fig. 3d). This was followed by extensive mineralization, particularly, in the veinlets-type W mineralization (Figs. 3a and 3b), and associated silicification and greisenization, forming assemblages of scheelite + wolframite + chalcopyrite + molybdenite + quartz + muscovite + fluorite ±K-feldspar ± plagioclase (Fig 4f). The quartz veins (type 3) always have greisen selvages ranging from centimeters to tens of centimeters. During the late stage of magmatic and hydrothermal evolution, low-temperature alteration minerals including dominantly calcite and minor quartz and chlorite were formed, which occur as veinlets crosscutting earlier-formed scheelite and sulfides .The paragenesis is illustrated in Fig. 5.

< Fig. 5 >

SAMPLES AND ANALYTICAL METHODS

Scheelite samples

Scheelite samples DHT-91, DHT-96, DHT-98, DHT-102, DHT-104 were taken from drills ZK11214 and ZK11612, and they are the veinlets-type scheelite (type 1) from the Neoproterozoic granite. Samples DHT-62 and DHT-138 are from the porphyritic granite associated with the type 1 mineralization, and DHT-131 and DHT-133 from the quartz vein-type mineralization (type 3). These samples were

prepared as polished sections for microprobe and laser ablation-inductively coupled plasma-mass spectrometric (LA-ICP-MS) analysis. Scheelite samples DHT-88, DHT-91, DHT-92, DHT-96, DHT-104, DHT-109, DHT-124, DHT-125, DHT-131, DHT-145, DHT-155 were selected for Sr-Nd isotope analysis.

Microprobe analysis

Major elements of scheelite were measured by wavelength-dispersive spectrometry at the MLR Key Laboratory of Metallogeny and Mineral Assessment, Chinese Academy of Geological Sciences, using a JEOL JXA8100 electron probe operating at an accelerating voltage of 15kVwith a 10nA beam current, 5 um beam spot, and 10-30s counting time. The following natural minerals and synthetic oxides were used for calibration: K-feldspar (K), jadeite (Na), olivine (Mg), apatite (Ca), cassiterite (Sn), CuO (Cu), hematite (Fe), MnO (Mn), scheelite (W), Cr_2O_3 (Cr), wulfenite (Mo) and rutite (Ti). All data were corrected using the ZAF procedures. The detection limit is 0.01% for most of the elements, but 0.02% for Mo and Ti.

LA-ICP-MS method

The LA-ICP-MS analysis was performed at the Key Laboratory of Orogenic Belts and Crustal Evolution, Peking University. Laser sampling was carried out using an ArF excimer laser ablation system (193 nm wavelength), connected to an Agilent 7500a ICP-MS with a 1 m transfer tube. Helium was used as carrier gas, and argon as the make-up gas and mixed with the carrier gas via a T-connector before entering the ICP. The carrier and make-up gas flows were optimized by ablating NIST SRM 610 to obtain maximum signal intensities while keeping low ThO/Th (0.1-0.3%) ratios to

reduce the oxide and doubly charged ion interferences. Each LA-ICP-MS analysis incorporated a ~20s background acquisition (gas blank) followed by a 60s data acquisition from the sample. Every tenth spot analysis was followed by one NIST SRM 610 analysis to correct the time-dependent drift of sensitivity and mass discrimination of the ICP-MS. Reference glasses (GSE, NIST612, NIST614) were analyzed prior to and after the sample measurements. The NIST SRM 610 were used as external standard and average CaO contents of scheelite were used as internal standard. The data were processed using Glitter software.

Cathodoluminescence (CL)

Mapping the distribution of trace elements within a single grain can help revealing the origin of fluids. Many such studies have been done on minerals such as zircon, carbonates, quartz and apatite (e.g., Marshall 1988; Shore and Fowler 1996). We used a cold cathodegenerator Gatan Chromal CL, the samples were photographed using a Quanta FEG 650 from FEI Corporation operated at about 12keV and with a spot 5.5 under a vacuum of approximately 30Pa at Peking University. The samples were photographed at 298 K.

Sr-Nd isotope analysis

About 100mg of scheelite were dissolved in a mixture of HNO_3+HF in a sealed Teflon beaker on a hot plate (80℃) for seven days. Separation and purification of Rb, Sr, Sm and Nd were done using a second cation-exchange column at the Key Laboratory of Orogenic Belts and Crustal Evolution, Peking University, conditioned and cleaned with dilute HCl as described by Chen et al. (2000). Isotopic analyses

were performed on a Thermo-Finnigan TRITON thermal ionization mass spectrometer (TIMS) at Tianjin Institute of Geology and Mineral Resources, China Geological Survey. Contents of Rb, Sr, Sm and Nd were measured using the isotope dilution method. The uncertainty in concentration analyses by isotope dilution is 2% for Rb, 0.5-1% for Sr, and <0.5% for Sm and Nd depending upon concentration levels. The Sr and Nd isotopic ratios were normalized against $^{86}Sr/^{88}Sr$ = 0.1194 and $^{146}Nd/^{144}Nd$ = 0.7219, respectively. During the period of data acquisition, Sr standard NBS-987 gave $^{87}Sr/^{86}Sr$ = 0.710231±0.000012(2σ), and LRIG Nd standard yielded $^{143}Nd/^{144}Nd$ = 0.512202 ± 0.000003(2σ). The BCR-2 standard, prepared with the same procedure as the samples, yielded Sm = 6.547 ppm, Nd = 28.799 ppm, $^{147}Sm/^{144}Nd$ = 0.1376, $^{143}Nd/^{144}Nd$=0.512624 ± 0.000003(2σ), Rb = 46.59 ppm, Sr = 330.11ppm, $^{87}Rb/^{86}Sr$ = 0.4076, and $^{87}Sr/^{86}Sr$ = 0.705050 ± 0.000005(2σ).

RESULTS

Major elements

Twelve major element analyses were conducted by the electron microprobe method on six scheelite samples from the Shimensi deposit (Table 1.3). The scheelites have CaO=19.7-20.1%, WO_3=79.9-80.3%, and MoO_3 = 0.01-0.06%. All the six scheelites have minor CuO, MnO, MgO, TiO_2, FeO, Na_2O and K_2O. As seen in Fig. 6, compared with the scheelites from other W deposits such as the King Island W deposit (Kwark and Tan 1981), the Kara W deposit (Zaw and Singoyi 2000) and the

skarn-type W-Mo deposits of the Baizhangyan and Jitoushan (Song et al. 2014), our samples have much lower concentrations of MoO_3.

< Table 1>

< Fig. 6 >

Cathodoluminescence (CL)

The $(WO_4)^{2-}$ group shows a characteristic broad emission peak, known as self-luminescence band (SB), which is attributed to electronic transitions in the molecular orbit (Grasser and Scharmann 1976). The position of this peak depends on the content of Mo which substitutes for W, and could shift from 425 nm (Mo-free scheelite with blue CL) to 530 nm (>1 wt% Mo with yellow CL; Tyson et al. 1988). Sharp peaks, or characteristic peaks, are related to REE^{3+} ions in substitution for Ca^{2+} in the scheelite lattice. Generally, the variation of CL colour of scheelite has a close relationship with the contents of Mo and REE (Cannon and Murata 1944; Kroger 1948; Kononov 1967; Shoji and Sasaki 1978; Brugger et al. 2000) and sometimes even a small change of the Mo content may lead to the change of CL colours. Besides, other factors such as vacancies, lattice distortions also can change the CL colour of scheelite. Owing to the lack of trace element analyses of scheelites by sensitive mapping techniques, the exact reason for the change of CL colour is unclear. However, considering the very low concentrations of Mo in our scheelites, the different CL colours may reflect variations of REE concentrations in scheelites (Brugger et al. 2000). CL images of our samples vary from red to blue and to yellow, and the blue CL is the most common. The scheelites with yellow CL images have the

highest REE concentrations (average ∑REE 999 ppm), and those with red CL images show the lowest REE (average ∑REE 249 ppm; Fig. 7). The scheelites with blue CL images have intermediate REE abundances (808 ppm).

The Eu anomalies of scheelites in the chondrite-normalized REE patterns probably have something to do with the CL images, although exact relationships between them remain unclear. As seen in Fig. 7, scheelites with yellow and red CL images show negative and positive Eu anomalies in the REE patterns, respectively, but those with blue CL images show both positive and negative Eu anomalies (origin of Eu anomalies discussed below) (Figs. 7d, 7e, 7f).

< Fig. 7 >

Trace elements

A total of 88 trace element analyses were carried out by the LA-ICP-MS method on 9 scheelites from the Shimensi deposit (Table 2). In addition, we obtained trace elements of one fluorite coexisting with scheelite (type 1) in the Neoproterozoic granite and of 16 analyses of wolframite crosscut by the late-stage scheelite in the quartz vein-type mineralization (type 3). Representative analyses are listed in Table 3. The chondrite-normalized REE patterns are shown in Fig 8. Scheelite samples from Shimensi have highly variable Sr (27.7-1581.6 ppm), Mo (0.41-294 ppm), Nb (2.5-751 ppm), and Ta (3.1-76.3 ppm). Other trace elements such as Rb, Ba, Ti, Cu, Sn, U, Th, Sc, Zr and Hf are negligible.

< Fig. 8 >

< Table 2 >

<Table 3 >

The ∑REE + Y abundances of scheelites range from 40 to 3394 ppm, but mostly exceed 400 ppm. The majority of the scheelite samples are characterized by LREE-enriched REE patterns with $(La/Yb)_N$ ranging from 1.1-137.4 (Fig. 8), but four scheelite samples show different REE patterns with $(La/Yb)_N$ in the range 0.61-0.78. Both negative and positive Eu anomalies appear in the samples, even within in a single grain. The δEu（$\delta Eu=Eu_N/(Sm_N\times Gd_N)^{1/2}$）values vary significantly, ranging from 0.12 to 12.8. Twenty nine analyses show negative Eu anomalies and 59 positive Eu anomalies. Scheelites from the veinles-type mineralization show both negative and positive Eu anomalies in the REE patterns (Figs. 8a, 8b, 8c), and those hosted in the quartz-vein type mineralization exhibit positive Eu anomalies (Fig. 8d). The fluorite coexisting with scheelite shows LREE-depleted REE patterns (Fig. 8e) and the wolframites exhibit obvious HREE-rich patterns (Fig. 8f).

Sr-Nd isotopes

The Nd and Sr isotopic data of the scheelites from the Shimensi deposit are shown in Table 4. They show large variation in Sm (2.24-81.3 ppm) and Nd (12.56-277.66 ppm), with $^{147}Sm/^{144}Nd$ = 0.0942-0.1770 and $^{143}Nd/^{144}Nd$ = 0.512176-0.512275, and the calculated initial Nd isotopic compositions $\varepsilon_{Nd}(t)$ = -6.1 to -8.1. The initial $^{87}Sr/^{86}Sr$ ratios of these scheelites are unusually high, ranging from 0.72305 to 0.76569.

<Table 4>

DISCUSSION

Substitution mechanisms of REE^{3+} for Ca^{2+} in scheelite

The substitution of trivalent REE for divalent Ca requires not only charge balance but also a modification of the crystal structure, particularly the size of the Ca site (Raimbault et al. 1993; Ghaderi et al. 1999). The following three mechanisms are proposed by Nassau and Loiacono (1963), Burt (1989) and Ghaderi et al. (1999).

$$2Ca^{2+} = REE^{3+} + Na^{+} \quad (1)$$

$$Ca^{2+} + W^{6+} = REE^{3+} + Nb^{5+} \quad (2)$$

$$3Ca^{2+} = 2REE^{3+} + \square Ca \quad (3)$$

Here □Ca is a Ca-site vacancy. Different substitution mechanisms will lead to different chondrite-normalized REE patterns of scheelites. The MREE-enriched REE patterns of scheelites are related to the substitution of $2Ca^{2+} = REE^{3+} + Na^{+}$, and the relatively flat chondrite-normalized REE patterns result from the substitution of $3Ca^{2+} = 2REE^{3+} + \square Ca$ (Ghaderi et al. 1999).

Ghaderi et al. (1999) suggested that a REE element with ionic radius close to 1.06 Å would preferentially substitute into the Ca site according to Equation 1 if Na is available providing the charge balance. Thus, the ore-forming fluid should be enriched in Na if scheelite shows MREE-rich REE patterns. Brugger et al. (2002) attributed the feature of MREE-enrichment of scheelite from hydrothermal gold deposits to substitution by mechanism #1. As shown in Fig 8, the scheelite samples of Shimensi display no MREE-enriched REE patterns, and the ore-forming fluids have low salinity (1%-9% NaCl; unpublished data). As shown in Fig 9a, all the scheelites of the Shimensi deposit show Na abundance much lower than $\sum$REE+Y. This

suggests that Equation 1 is less likely to be the major substitution mechanism for the REE patterns of scheelite.

< Fig. 9 >

Equation 2 requires that scheelites are rich in Nb^{5+} and have Nb abundances close to the total REEs. Dostal et al. (2009) suggest that this substitution is responsible for the scheelites of the Nova Scotia deposit, based on the positive correlation between Nb^{5+} and $Nd^{3+}$of scheelites. The Shimensi scheelites, however, contain Nb contents of 2.5-751 ppm (mostly <60 ppm), which is much lower than their REE contents (9.9-2548 ppm; Table 3). This, together with the absence of a positive correlation between Nb^{5+} and $\sum$REE in most scheelites (Fig. 9b), suggests that Equation 2 is also not the major substitution mechanism.

The Shimensi scheelites are characterized by low Na and Nb, and relatively high total REE abundances. The average Na+Nb concentrations account for 13.56% of $\sum$ REE+Y in scheelite hosted in the Mesozoic porphyritic granite and 12.19% for scheelite from the Neoproterozoic granite. Besides, the scheelites of Shimensi deposit show no MREE-enriched REE patterns. So, both the substitutions of Na + REE and Nb + REE for Ca are not the principle mechanism for the scheelites in the Shimensi deposit. The REE patterns could be best interpreted by the substitution mechanism of Equation 3, in which REE ions substitute into the structure in pairs, associated with a vacant Ca site. It follows from Coulomb's law that the energy level for this substitution is minimized when the vacant Ca site lies between the two REE-substituted sites. The presence of such a vacancy adjacent to the REE sites

allows them to be flexible so that they can incorporate REE of any size (Ghaderi et al. 1999). Considering there is no priority for REE elements to substitute into Ca^{2+}, the scheelites can record the REE characteristics of ore-forming fluids.

Europium anomalies in the chondrite-normalized REE patterns

Some scheelites show negative Eu anomalies in the chondrite-normalized REE patterns, while others show positive Eu anomalies; the two were observed in a single grain with compositional zoning (Figs. 8a and 8b). As shown in Fig. 10a, data points of the scheelites hosted in the Mesozoic porphyritic granite roughly plot along the dashed-line, suggesting that Eu is dominated by Eu^{3+}, which is consistent with the mostly negative Eu anomalies of these scheelites. The Eu abundances of scheelites hosted in the Neoproterozoic granite and in the quartz veins, however, show no correlations with Eu^*_N, suggesting the dominance of Eu^{2+} in the ore-forming fluid, which agrees with the dominance of positive Eu anomalies in these scheelites. Since Eu^{2+} is commonly thought to enter more readily the Ca site in scheelite than Eu^{3+}, a positive Eu anomaly is expected when $Eu^{2+} >> Eu^{3+}$ in the fluid. If Eu^{3+} is dominant in the fluid, it behaves like other REE^{3+}, and thus resulting in no change in the size of Eu anomaly (Ghaderi et al., 1999).

As discussed before, REEs enter the lattice of scheelite by mechanism of $3Ca^{2+} = 2REE^{3+} + \square Ca$, crystallochemical control of REE entrance (with Na) is not important. This is supported by the non-correlation between Na and δEu for the scheelites from both the porphyritic granites and quartz vein, because otherwise abundance of Eu^{3+} and thus lower δEu values and negative correlation between δEu and Na would be

observed in these scheelites (Fig. 10b). However, a slightly negative correlation between Na and δEu is seen for scheelites from the Neoproterozoic granite, suggesting partial substitution of REE + Na for 2Ca (equation 1, see before). We think such a substitution is not important, because the abundance of Na (average 107 ppm) is much lower than that of REE in scheelite (average 902 ppm).

Eu anomalies (δEu) may be inherited from the parent hydrothermal fluids or arise from a change in oxidation state (Eu^{2+} vs. Eu^{3+}) of the dissolved Eu. Mo enters the scheelite lattice as Mo^{6+} by substituting for W^{6+} under oxidized conditions, whereas Mo contents of scheelite decrease if molybdenite (host of Mo) precipitates under reduced conditions. One Raman spectrum was done for fluid inclusions in quartz coexisting with scheelite as shown in Fig. 4d. The spectrum reveals that CH_4 is common in the inclusions, and a reduced fluid is inferred for the tungsten mineralization. Besides, as shown in Fig. 6, the Mo concentrations of our samples are much lower than those of the scheelites from several other W deposits (e.g., King Island, Kara, Jitoushan and Baizhangyan), suggesting that they precipitated from strong reduced fluids. This means that the fO_2 of ore-forming fluids appears to show no significant variation throughout the ore-forming processes, and thus the Eu anomalies are probably driven by parent fluids and not by the oxido-reduction conditions/changes. Therefore, the Eu anomalies and REE patterns of the scheelites could record features of ore-forming fluids.

< Fig. 10 >

Source and evolution of ore-forming fluids and metals

The ore-forming fluids could have been originated from the nearby Mesozoic porphyritic granite, the Shuangqiaoshan group meta-sedimentary rocks (metamorphic fluid), and from mixing of meteoric water. Our data suggest that the ore-forming fluids are mainly derived from the exsolution of magmatic fluids, but compositionally modified during a late-stage fluid-rock interaction. Main arguments for this are as below.

First, the REE (and other trace elements) abundance of scheelites could reflect the nature and evolution of ore-forming fluid, and scheelites (DHT-138) from the Mesozoic porphyritic granite and those (DHT-102,104) from the Neoproterozoic granite (veinlets-type) are chosen for such a study. Scheelites from DHT-138 show complicated chondrite-normalized REE patterns with both positive and negative Eu anomalies (Fig. 8a), whereas those from DHT-102 and DHT-104 show simple REE patterns, mostly with positive Eu anomalies (Figs. 8b and 8c). The scheelites from DHT-138 with negative Eu anomalies could represent the primitive ore-forming fluids exsolved from the porphyritic granite, which have higher concentrations of ∑REE and Nb+Ta, but lower Sr (Figs.11a-11c) than those with positive Eu anomalies. When the ore-forming fluids flew upward into the cracks in the Neoproterozoic granite, the concentrations of ∑REE, Nb, Ta decreased gradually with the decline of temperature and pressure. With increasing fluid/rock ratios, more and more plagioclase in the Neoproterozoic granite were altered to sericite, providing significant amounts of Ca, Eu and Sr for the hydrothermal fluids to form scheelite. Meanwhile, biotite was altered to chlorite, providing Fe^{2+} for the formation of wolframite. The ratios of

Eu^{3+}/Eu^{2+} in the evolved hydrothermal fluids could decrease gradually with alteration of plagioclase (supplying Eu^{2+}), as indicated by a shift from low δEu values (0.12) of the scheelites from the porphyritic granite to high ones (12.8) of the scheelites from the Neoproterozoic granite. Therefore, the scheelites precipitated in an evolved fluid show high concentration of Sr, positive Eu anomalies and low ∑REE, Nb, Ta (Fig. 10d and Figs. 11a-11c). Similar phenomenon occurs in sample DHT-102 (Figs. 11d-11f).

This model is consistent with the fact that the scheelites from DHT-104 (farther from the porphyritic granite than DHT-102) show positive Eu anomalies, while those from DHT-102 show both positive and negative Eu anomalies in the REE patterns (Figs. 8b and 8c). The fluid evolution was also reflected by the compositional zoning in a single scheelite. As shown in Fig. 8b, the center part of scheelite from DHT-102 shows negative Eu anomalies in the REE patterns, while the rim of the same scheelite shows positive Eu anomalies, suggesting that the center and rim scheelites were precipitated from an earlier (with more contribution from the magmatic fluids) and later-stage fluids (with more contribution from surrounding rocks), respectively. Thus, we attribute the variation of REE (and other trace elements) and Eu anomalies of the ore-forming fluids of the veinlets-type mineralization to possible interaction of the magmatic fluids with country rocks during the process of fluid evolution, which evolved from the primary fluids exsoluted from the porphyritic granite to the late-stage fluids in the cracks of the Neoproterozoic granite.

The scheelites (DHT-131 and DHT-133) from the quartz vein-type mineralization,

however, show the lowest abundance of REE+Y, high Sr (Fig. 8d; Fig. 10d), and exclusively positive Eu anomalies (δEu =1.52-7.40) in the REE patterns, which we believe could have precipitated in a final stage of the mineralization in the Shimensi ore deposit. The significant decrease of REE contents shown by the scheelites from this mineralization could have been caused by two factors. One is the precipitation of REE-rich fluorite and wolframite (Goldmann et al. 2013), and the other is mixing of meteoric water, which is inferred from the low oxygen isotopes of quartz ($\delta^{18}O_{H2O}$ = 4.5‰-7.3‰) and wolframite (3.8‰-6.3‰) from the scheelite-bearing quartz veins (Wang et al. 2015). The δEu variation could also be attributed to mixing of meteoric water and/or metamorphic fluid as suggested by Brugger et al. (2002). However, meteoric waters normally show very low REE contents, which could cause a decrease of REE contents of ore-forming fluid by dilution, but cannot change the Eu anomalies significantly. Mixing of metamorphic fluids from the Shuangqiaoshan group metasedimentary rocks in the ore-forming fluid cannot be precluded, but involvement of such a metamorphic fluid is less likely to have caused the positive Eu anomalies in evolved ore-forming fluid, because the meta-sedimentary rocks are characterized by significant negative Eu anomalies (δEu=0.36-0.87) in the chondrite-normalized REE patterns (Zhang et al. 2012). In addition, precipitation of fluorite and wolframite from the ore-forming fluid appears to have not exerted significant impact on Eu anomalies, because the two minerals show minor Eu anomalies in the REE patterns (Figs. 8e and 8f).

< Fig. 11 >

Second, the isotopic data of scheelite can shed lights on the source of ore-forming fluids (Bell et al. 1989). Previous studies of REE behavior during hydrothermal processes (e.g., Farmer and DePaolo 1987; Lottermoster 1991; DePaolo and Getty 1996) have shown that Nd is of low abundance and is mostly immobile. Therefore, the Nd isotopes of scheelite can record the characteristics of the fluid sources. The scheelite from the Shimensi deposit shows a low and narrow range of $\varepsilon_{Nd}(t)$ values from -6.1 to -8.1, similar to those of the Mesozoic porphyritic granite (-5.1 to -8.6; Fig. 12a). This suggests that porphyritic granite could be an important source for the ore-forming fluids. This agrees with the REE data of scheelites. The scheelites from the dominant veinlets-type mineralization typically show negative Eu anomalies in the chondrite-normalized REE patterns (Fig. 8a), suggesting that the ore-forming fluid may have come from the Mesozoic porphyritic granite that exhibits significant negative Eu anomalies in the REE patterns (Figs. 8a). This is also supported by the occurrence of fluorite in the veinlets-type W-mineralization (Figs. 7a and 7b), because, as shown in Fig. 7a, the porphyritic granite is a fluorine-rich system as evidenced by the common presence of fluorite (enclosed in plagioclase) of magmatic origin. However, fluorite is absent in the Neoproterozoic granite, suggesting that fluorine in the ore-forming fluids originated mainly from the porphyritic granite.

Nd isotopes cannot be used to decipher between the Mesozoic granite and the Shuangqiaoshan Group metasediments, because the granites were originated from partial melting of high-grade metamorphic lower crustal rocks analogous to the Shuangqiaoshan Group (Huang and Jiang 2014; Mao et al. 2014), and the Sm/Nd

ratio of the lower crustal rocks is expected to maintain unchanged during the process of high-grade metamorphism. This is consistent with the similarity of Nd isotopic compositions of the granites and Shuangqiaoshan group rocks (Fig. 12a). The Sr isotopic data, however, could be used to solve the issue, because the Rb/Sr ratios of the high-grade metamorphic lower crustal metasediments are expected to decrease significantly compared to the Shuangqiaoshan group metasediments due to preferential release of Rb relative to Sr during the high-grade metamorphism, and thus less radiogenic Sr isotopes are developed in the lower crustal rocks. Sr is mobile during hydrothermal processes, and could be used to trace the fluid evolution path (Voicu et al. 2000). There are lines of evidence from porphyry copper and orogenic gold deposits that the $^{87}Sr/^{86}Sr$ of fluid can be modified significantly within 100m after flowing across a contact between isotopically different wall rocks (Böhlke and Kistler 1986; Farmer and DePaolo 1987). The scheelites from the Shimensi deposit show unusually high initial $^{87}Sr/^{86}Sr$ ratios (I_{Sr}) of 0.7231-0.7657 (Table 4), which are significantly higher than those of the three types of Mesozoic granitoids (0.7210-0.7365; Mao et al. 2014) and those of many other S-type granites worldwide, e.g., the Mesozoic granites in South China (0.705-0.730; Chen and Jahn 1998; Fig. 12a), and the S-type granites from the Lachlan Fold Belt with Sr isotopic ratios in the range 0.708 to 0.720 (Chappell and White 1992). Therefore, additional source of radiogenic ^{87}Sr is required to account for the Sr isotopic compositions of the Shimensi scheelites. There are two candidates for such a source: one is the Neoproterozoic granitoids, and the other the Shuangqiaoshan Group rocks; both are the host rocks of

the ore-bearing quartz veinlets. As shown in Fig. 12a, the Neoproterozoic granitoids are less likely to be responsible for the elevated Sr isotopic ratios of the scheelites, since these granitoids have Sr isotopic ratios <0.731 if calculated at the formation age (143 Ma) of scheelites (Wu et al. 2006). We think that the low-grade meta-sedimentary rocks of the Shuangqiaoshan Group could be such a source, because they contain abundant Rb-rich micas and thus have radiogenic Sr (with I_{Sr} ratios up to 0.7594; Ma and Xiang 1993; Chen and Jahn 1998; Li et al. 2003; Zhang et al. 2012). Interaction of the ore-forming fluids derived from the porphyritic granites with the Shuangqiaoshan Group rocks would introduce additional radiogenic ^{87}Sr and significantly elevate the Sr isotopic ratios of the fluids, from which scheelites precipitated. A calculation using the simple two-components mixing model suggests that contribution from the Shuangqiaoshan Group is about 30% for most scheelites, but two scheelite samples (with I_{Sr}>0.75) may have been originated mainly from the Shuangqiaoshan group meta-sediments. Although the meta-sedimentary rocks of the Shuangqiaoshan Group are not seen around the Shimensi deposit, they are distributed widespread in the Jiangnan orogenic belt, and could dominate the middle to lower crust of study area as suggested by the consistency of the Sr-Nd isotopic compositions of the Mesozoic granites with those of the Shuangqiaoshan Group rocks. The meta-sedimentary rocks can be seen ca. 2 km to the south of the Shimensi deposit, where a tungsten-bearing granite pluton occurs (the Shiweidong pluton; Fig. 2a).

< Fig. 12 >

A plot of $^{87}Sr/^{86}Sr$ vs Nb+Ta (Fig. 12b) was used to further trace the evolution of the ore-forming fluids. According to the limited data, the scheelites hosted in the Neoproterozoic granite (away from the porphyritic granites) show higher Sr isotopic ratios and lower contents of Nb, Ta than that hosted in the Mesozoic porphyritic granite, suggesting more contribution from the Shuangqiaoshan group metasediments in the evolved ore-forming fluids. One scheelite hosted in the Neoproterozoic granite shows a low Sr isotopic ratio (Fig. 12b), which may be less affected by the Shuangqiaoshan Group rocks. The different types of scheelites show roughly the same Nd isotopic compositions ($\varepsilon Nd(t)$ = -7.5 to -8.1) and no correlation with Nb+Ta contents (not shown). This again suggests that the Shuangqiaoshan sedimentary rocks could have contributed to the ore-forming fluids (and metals as well), particularly, in a late-stage of ore-formation.

Possible origin of tungsten include: (1) the porphyritic granites, from which W metals were exsoluted along with the ore-forming fluids, as supported by the presence of magmatic scheelite grain enclosed in plagioclase (Fig. 7a) and by the much higher concentration of W in the porphyritic granite (22.4 ppm) than in average continental crust (1 ppm; Rudnick and Gao 2003), and (2) the Shuangqiaoshan group meta-sedimentary rocks with high W contents (average 11.8 ppm; Liu et al. 1982), from which W could have been leached into the ore-forming fluids via fluid-rock interaction as stated before. The Neoproterozoic granite is less likely to be the source of ore-forming metals, because no W deposits were seen at the contacts between the Neoproterozoic granite and Shuangqiaoshan group rocks.

Tungsten and ore-forming fluids of most tungsten deposits associated with granites were generally considered to have originated from the granite itself (Reyf 1997; Audétat et al. 2000; Webster et al. 2004; Thomas et al. 2005). The Shimensi tungsten deposit is traditionally thought to have formed as a result of fluid (along with tungsten) exsolution only from the porphyritic granites (Huang and Jiang 2014; Mao et al. 2014). Our new data, especially the unusually high initial $^{87}Sr/^{86}Sr$ ratios (I_{Sr}) of scheelites (Fig 12a), indicate that the country-rocks Shuagqiaoshan Group also contributed a lot to the ore forming fluids and metals in the Shimensi deposit.

IMPLICATIONS

Our data reveal that $3Ca^{2+}=2REE^{3+}+\square Ca$ (where $\square Ca$ is a Ca-site vacancy) could be the principal substitution mechanism responsible for Ca^{2+} substitution by REE in scheelite of the Shimensi deposit. Combined trace elements and CL images of scheelites suggest that the complex REE_N patterns and the variably positive and negative Eu anomalies record the evolution of the ore-forming fluids. We suggest that the scheelites hosted in Mesozoic porphyritic granite showing negative Eu anomalies represent a primitive ore-forming fluids, and the scheelites hosted in the Neoproterozoic granite showing positive Eu anomaly were precipitated from an evolved ore-forming fluids. The low concentrations of Mo indicate that scheelites precipitated under reducing conditions and the variation of Eu anomalies were not caused by changing redox conditions. The negative Eu anomalies of scheelites were inherited from the porphyritic granite, whereas the positive Eu anomalies in scheelites

were caused by alteration of plagioclase from country rocks with increasing fluid/rock ration. The variation of the contents of ∑REE, Nb, Ta and Sr also reflect the evolution of ore-forming fluids. The Sr-Nd isotope data of scheelites from the Shimensi deposit show that both the Mesozoic porphyritic granite and the Neoproterozoic Shuangqiaoshan group rocks have contributed metals to the ore-forming fluids.

Acknowledgments

Zhu Wenping and Ma Fang are thanked for their kind assistance in isotopic and trace element analyses, respectively. This paper is financially supported by a grant from the Natural Science Foundation of China (#41272067). We are very grateful to Prof Christian Marignac, Frank Melcher and Julien Mercadier (the Editor) for their constructive comments that lead to significant improvement of the manuscript.

REFERENCES CITED

Allen, C.C., and Folinsbee, R.E. (1944) Scheelite veins related to porphyry intrusives, Hollinger Mine. Economic Geology. 39, 340-348.

Audétat, A., Günther, D., and Heinrich, C.A. (2000) Magmatic-hydrothermal evolution in a fractionating granite: A microchemical study of the Sn-W-F-mineralized Mole Granite (Australia). Geochimica et Cosmochimica Acta. 64, 3373-3393.

Bell, K., Anglin, C.D., and Franklin, J.M. (1989) Sm-Nd and Rb-Sr isotope systermatics of scheelites: Possible implications for the age and genesis of

vein-hosted gold deposits. Geology, 17, 500-504.

BGMRJX (Jiangxi Bureau of Geology and Mineral Resources). (1984) Regional geology of Jiangxi province. Geological Publishing House, 224 p.

Böhlke, J.K., and Kistler, R.W. (1986) Rb-Sr, K-Ar, and stable isotope evidence for the ages and sources of fluid components of gold-bearing quartz veins in the northern Sierra Nevada Foothills metamorphic belt, California. Economic Geology, 81, 296-322.

Brugger, J., Bettiol, A.A., Costa, S., Lahaye, Y., Bateman, R., Lambert, D.D., and Jamieson, D.N. (2000) Mapping REE distribution in scheelite using luminescence. Mineralogical Magazine, 64, 891-903.

Brugger, J., Mass, R., Lahaye, Y., Mcrae, C., Ghaderi, M., Costa, S., Lambert, D., Bateman, R., and Prince, K. (2002) Origins of Nd–Sr–Pb isotopic variations in single scheelite grains from Archaean gold deposits, Western Australia. Chemical Geology, 182, 203-225.

Brugger, J., Etschmann, B., Pownceby, M., Liu, W., Grundler, P., and Brewe, D. (2008) Oxidation state of europium in scheelite: Tracking fluid–rock interaction in gold deposits. Chemical Geology, 257, 26-33.

Burt, D.M. (1989) Compositional and phase relations among rare earth elements. Reviews in Mineralogy, 21, 259-307.

Cannon, R.S., and Murata, K.J. (1944) Estimating molybdenum content of scheelite or Calcium tungstate by visual color of its fluorescence. U.S. Patent 2, 346661.

Chappell, B.W., and White, A.J.R. (1992) I-and S-type granites in the Lachlan Fold

Belt. Transactions of the Royal Society of Edinburgh: Earth Sciences, 83, 1-26.

Charvet, J., Shu, L.S., Faure, M., Choulet, F., Wang, B., Lu, H.F., and Le Breton, N. (2010) Structural development of the Lower Palaeozoic belt of South China: genesis of an intracontinental orogeny. Journal of Asian Earth Sciences, 39, 309-330.

Charvet, J. (2013) The Neoproterozoic-Early Paleozoic tectonic evolution of the South China Block: an overview. Journal of Asian Earth Sciences, 74, 198-209.

Chen, B., Jahn, B.M., Wilde, S., and Xu, B. (2000) Two contrasting Paleozoic magmatic belts in northern Inner Mongolia, China: petrogenesis and tectonic implications. Tectonophysics, 328, 157-182.

Chen, J.F., and Jahn, B.M. (1998) Crustal evolution of southeastern China: Nd and Sr isotopic evidence. Tectonophysics, 284, 101-133.

Cottrant, J.F. (1981) Cristallochimie et géochimie des terres rares dans la scheelite: Application à quelques gisements francais. Ph.D. thesis, University of Paris-VI, France.

Darbyshire, D.P.F., Pitfield, P.E.J., and Campbell, S.D.G. (1996) Late Archean and Early Proterozoic gold-tungsten mineralization in the Zimbabwe Archean craton: Rb-Sr and Sm-Nd isotope constrains. Geology, 24, 19-22.

Deer, W.A., Howie, R.A., and Zussman, J. (1966) An Introduction to the Rock Forming Minerals, 515 p. Longman Press, New York.

Deng, Z.B., Liu, S.W., Zhang, L.F., Wang, Z.Q., Wang, W., Yang, P.T., Luo, P., and Guo, B.R. (2014) Geochemistry, zircon U-Pb and Lu-Hf isotopes of an Early

Cretaceous intrusive suite in northeastern Jiangxi Province, South China Block: Implications for petrogenesis, crust/mantle interactions and geodynamic processes. Lithos, 200, 334-354.

DePaolo, D.J., and Getty, S.R. (1996) Models of isotopic exchange in reactive fluid-rock systems: implications for geochronology in metamorphic rocks. Geochimica et Cosmochimica Acta, 60, 3933-3947.

Dostal, J., Kontak, D.J., and Chatterjee, A. (2009) Trace element geochemistry of scheelite and rutile from metaturbidite-hosted quartz vein gold deposits, Meguma Terrane, Nova Scotia, Canada: Genetic implications. Mineralogy and Petrology, 97, 95-109.

Eichhorn, R., Holl, R., Jagoutz, E., and Schrer, U. (1997) Dating scheelite stages: A strontium, neodymium, lead approach from the Felbertal tungsten deposit, Central Alps, Austria. Geochimica et Cosmochimica Acta, 61, 5005-5022.

Farmer, G.L., and DePaolo, D.J. (1987) Nd and Sr isotope study of hydrothermally altered granite at San Manuel, Arizona: implications for element migration paths during the formation of porphyry copper ore deposits. Economic Geology, 182, 1142-1151.

Feng, C.Y., Zhang, D.Q., Xiang, X.K., Li, D.X., Qu, H.Y., Liu, J.N., and Xiao, Y. (2012) Re-Os isotopic dating of molybdenite from the Dahutang tungsten deposit in northwestern Jiangxi Province and its geological implication. Acta Petroligica Sinica, 28, 3858-3868.

Frei, R., Nagler, T.F., Schonberg, R., and Kramers, J.D. (1998) Re-Os, Sm-Nd, U-Pb,

and stepwise lead leaching isotope systematics in shear-zone hosted gold mineralization- genetic tracing and age constrains of crustal hydrothermal activity. Geochimica Cosmochimica Acta, 62, 1925-1936.

Ghaderi, M., Palin, J. M., Campbell, I. H., and Sylvester, P. J. (1999) Rare earth element systematics in scheelite from hydrothermal gold deposits in the Kalgoorlie-Norseman region, Western Australia. Economic Geology, 94, 423-437.

Goldmann, S., Melcher, F., Gäbler, H.E., Dewaele, S., De Clercq, F., and Muchez, P. (2013) Mineralogy and trace element chemistry of ferberite/reinite from tungsten deposits in central Rwanda. Minerals, 3, 121-144.

Grasser, R., and Scharmann, A. (1976) Luminescent sites in $CaWO_4$ and $CaWO_4$: Pb crystals. Journal of Luminescence, 12-13, 473-478.

Huang, L.C., and Jiang, S.Y. (2014) Highly fractionated S-type granites from the giant Dahutang tungsten deposit in Jiangnan Orogen, Southeast China: geochronology, petrogenesis and their relationship with W-mineralization. Lithos, 202-203, 207-226.

Kempe, U., Belyatsky, B., Krymsky, R., Kremenetsky, A., and Ivanov, P. (2001) Sm–Nd and Sr isotope systematics of scheelite from the giant Au (–W) deposit Muruntau (Uzbekistan): implications for the age and sources of Au mineralization. Mineralium Deposita, 36,379-392.

Kent, A.J.R., Campbell, I.H., and McCulloch, M.T. (1995) Sm-Nd systematics of hydrothermal scheelite from the Mount Charlotte mine, Kalgoorlie, Western

Australia: An isotopic link between gold mineralization and komatiites. Economic Geology, 90, 2329-2335.

Kononov, O.V. (1967) Photoluminescence characteristics of molybdenum-bearing scheelites. Doklady Akademiia Nauk SSSR. 175, 120-123.

Kroger, F.A. (1948) Some aspects of the luminescence of solids. Elsevier, New York.

Kwak, T.A.P., and Tan, T.H. (1981) The geochemistry of zoning in skarn minerals at the King Island (Dolphin) mine. Economic Geology, 76, 468-497.

Li, X.H., Li, Z.X., Ge, W.C., Zhou, H.W., Li, W.X., Liu, Y., and Wingate, M.T.D. (2003) Neoproterozoic granitoids in South China: crustal melting above a mantle plume at ca. 825 Ma? Precambrian Research, 122, 45-83.

Liu, Y.J., Li, Z.L., and Ma, D.S. (1982) The geochemical studies of tungsten-bearing formation in South China. Science in China (Series B), 10, 939-950.

Liu, Y.J. (1997) Rocks and formations in Jiangxi province, 381 p. China University of Geosciences press, Wuhan.

Liu, Y.S., and Ma, D.S. (1987) Geochemistry of Tungsten, 217 p. Science Press, Beijing. (in Chinese).

Lottermoser, B.G. (1991) Rare-earth elements and hydrothermal ore formation. Ore Geology Reviews, 7, 25-41.

Mao, Z.H., Cheng, Y.B., Liu, J.J., Yuan, S.D., Wu, S.H., Xiang, X.K., and Luo, X.H. (2013) Geology and molybdenite Re–Os age of the Dahutang granite-related veinlets-disseminated tungsten ore field in the Jiangxi Province, China. Ore Geology Reviews, 53, 422-433.

Mao, Z.H., Liu, J.J., Mao, J.W., Deng, J., Zhang, F., Meng, X.Y., Xiong, B.K., Xiang, X.K., and Luo, X.H. (2014) Geochronology and geochemistry of granitoids related to the giant Dahutang tungsten deposit, middle Yangtze River region, China: Implications for petrogenesis, geodynamic setting, and mineralization. Gondwana Research. doi:10.1016/j.gr.2014.07.005

Marshall, D.J. (1988) Cathodoluminescence of geological materials, 146 p. Unwin Hyman, Boston.

Ma, X., and Xiang, X.K. (1993) Preliminary study of the Nd isotopic model ages of the Precambrian metamorphic stratum in northeastern Jiangxi Province. Scientia Geologica Sinica, 28, 145-150.

Mueller, A.G., Laeter, J.R.D., David, I., and Groves, D.I. (1991) Strontium isotope systematics of hydrothermal minerals from epigenetic Archean gold deposits in the Yilgarn Block, Western Australia. Economic Geology, 86, 780-809.

Nassau, K., and Loiacono, G.M. (1963) Calcium tungstate-III: trivalent rare earth substitution. J Phys Chem Solids, 24, 1503-1510.

Noble, S., Spooner, E.T.C., and Harris, F. (1984) The Logtung large tonnage, low-grade W (scheelite)-Mo porphyry deposit, south-central Yunkon Territory. Economic Geology, 79, 848-868.

No. 916 Geological Team, Jiangxi Bureau of Geology, Mineral Resources, Exploration and Development. (2012) The Exploration Report of the Shimensi, North Portion of the Dahutang Tungsten Deposit, Wuning County, Jiangxi Province. Jiangxi Jutong Mining Corporation, 224 p.

Peng, J.T., Hu, R.Z., Zhao, J.H., and Fu, Y.Z. (2003) Scheelite Sm-Nd dating and quartz Ar-Ar dating from Woxi Au-Sb-W deposit western Hunan. Chinese Science Bulletin, 48, 2640-2646.

Raimbault, L., Baumer, A., Dubru, M., Benkerrou, C., Croze, V., and Zahm, A. (1993) REE fractionation between scheelite and apatite in hydrothermal conditions. American Mineralogist, 78, 1275-1285.

Reyf, F.G. (1997) Direct evolution of W-rich brines from crystallizing melt within the Mariktikan granite pluton, west Transbaikalia. Mineralium Deposita, 32, 475-490.

Roberts, S., Palmer, M.R., and Waller, L. (2006) Sm-Nd and REE characteristics of tourmaline and scheelite from the Bjorkdal gold deposit, northern Sweden. Evidence of an intrusion-related gold deposit? Economic Geology, 101, 1415 - 1425.

Rösler, H.J., Baumann, L., and Jung, W. (1968) Post magmatic mineral deposits of the northern edge of the Bohemian Massif: 23th Inter. Geol. Congress, Prague, Guide to Excursions 22 AC, 57 p.

Rudnick, R.L., and Gao, S. (2003) Composition of the continental crust. In: Rudnick RL (ed). Treatise on Geochemistry, 64 p. New York.

Shoji, T., and Sasaki, N. (1978) Fluorescent color and x-ray powder data of synthesized scheelite-powellite series as guides to determine its composition. Mining Geology, 28, 397-404.

Shore, M., and Fowler, A.D. (1996) Oscillatory zoning in minerals: a common

phenomenon. Canadian Mineralogist, 34, 1111-1126.

Shu, L.S., and Charvet, J. (1996) Kinematics and geochronology of the Proterozoic Dongxiang-Shexian ductile shear zone: With HP metamorphism and ophiolitic mélange (Jiangnan region, south China). Tectonophysics, 267, 291-302.

Song, G.X., Qin, K.Z., Li, G.M., Evans, N.J., and Chen, L. (2014) Scheelite elemental and isotopic signatures: Implications for the genesis of skarn-type W-Mo deposits in the Chizhou Area, Anhui Province, Eastern China. American Mineralogist, 99, 303-317.

Sun, S.S., and McDonough, W.F. (1989) Chemical and isotopic systematics of oceanic basalts: implications for mantle composition and processes. In A.D. Saunders and M.J. Norry, Eds., Magmatism in the Ocean Basins. Geological Society of London, Special Publication 42, U.K, 313-345.

Thomas, R., Förster, H.J., Rickers, K., and Webster, J.D. (2005) Formation of extremely F-rich hydrous melt fractions and hydrothermal fluids during differentiation of highly evolved tin-granite magmas: a melt/fluid-inclusion study. Contrib Mineral Petrol, 148, 582-601.

Tomschi, H.P., Oberthür, T., Saager, R., and Kramers, J. (1986) Geochemical and mineralogical data on the genesis of the Mazowe gold field in the Harare Bindura greenstone belt, Zimbabwe [ext. abs]. Geocongress'86, Johannesburg, South Afica, 1986, Extended Abstracts, 345-348.

Tyson, R.M., Hemphill, W.R., and Theisen, A.F. (1988) Effect of W:Mo ratio on the shift of excitation and emission spectra in the scheelite-powellite series.

American Mineralogist, 73, 1145-1154.

Uspensky, E., Brugger, J., and Graeser, S. (1998) REE geochemistry systematics of scheelite from the Alps using luminescence spectroscopy: from global regularities to local control. Schweizerische Mineralogische and Petrographische Mitteilungen, 78, 33-56.

Voicu, G., Bardoux, M., Stevenson, R., and Jebrak, M. (2000) Nd and Sr isotope study of hydrothermal scheelite and host rocks at Omai, Guiana Shield: implications for ore fluid source and flow path during the formation of orogenic gold deposits. Mineralium Deposita, 35, 302-314.

Wang, H., Feng, C.Y., Li, D.X., Xiang, X.K., and Zhou, J.H. (2015) Sources of granitoids and ore-forming materials of Dahutang tungsten deposit in northern Jiangxi Province: Constrains from mineralogy and isotopic tracing. Acta Petrologica Sinica, 31, 725-739.

Wang, J., and Li, Z.X. (2003) History of Neoproterozoic rift basins in South China: Implications for Rodinia break-up. Precambrian Research, 122, 141-158.

Wang, J., Zhou, X.L., Deng, Q., Fu, X.G., Duan, T.Z., and Guo, X.M. (2014) Sedimentary successions and the onset of the Neoproterozoic Jiangnan sub-basin in the Nanhua rift, South China. International Journal of Earth Science (Geologische Rundschau): doi 10.1007/s00531-014-1107-5.

Wang, R.C., Zhu, J.C., Zhang, W.L., Xie, L., Yu, A.P., and Che, X.D. (2008) Ore-forming mineralogy of W-Sn granites in the Nanling Range: Concept and case study. Geological Journal of China Universities, 14, 485-495.

Wang, X.L., Zhou, J.C., Griffin, W.L., Zhao, G.C., Yu, J.H., Qiu, J.S., Zhang, Y.J., and Xing. G.F. (2014) Geochemical zonation across a Neoproterozoic orogenic belt: Isotopic evidence from granitoids and metasedimentary rocks of the Jiangnan orogeny, China. Precambrian Research, 242, 154-171.

Wang, Y.J., Fan, W.M., Zhang, G.W., and Zhang, Y.H. (2013) Phanerozoic tectonics of the South China Block: key observations and controversies. Gondwana Research, 23, 1273-1305.

Webster, J., Thomas, R., Förster, H.J., Seltmann, R., and Tappen, C. (2004) Geochemical evolution of halogen-enriched granite magmas and mineralizing fluids of the Zinnwald tin-tungsten mining district, Erzgebirge, Germany. Mineralium Deposita, 39, 452-472.

Wu, R.X., Zheng, Y.F., Wu, Y.B., Zhao, Z.F., Zhang, S.B., Liu, X.M., and Wu, F.Y. (2006) Reworking of juvenile crust: Element and isotope evidence from Neoproterozoic granodiorite in South China. Precambrian Research, 146, 179-212.

Xu, K.Q. (1957) Finding of skarn Ca-W deposit in Yaogangxian W-Mn-Fe mine in Hunan Province and the genesis relation between the two kinds of deposits. Acta Geological Sinica, 2, 117-151.

Yao, J.L., Shu, L.S., Santosh, M., and Li, J.Y. (2013) Geochronology and Hf isotope of detrital zircons from Precambrian sequences in the eastern Jiangnan orogeny: constraining the assembly of Yangtze and Cathaysia Blocks in South China. Journal of Asian Earth Sciences, 74, 225-243.

Zaw, K., and Singoyi, B. (2000) Formation of magnetite-scheelite skarn mineralization at Kara, Northwestern Tasmania: evidence from mineral chemistry and stable isotopes. Economic Geolgoy, 95, 1215-1230.

Zhang, Y.J., Liao, S.B., Zhou, X.H., Yang, J., Yu, M.G., Jiang, R., Zhao, X.L., Chen, Z.H., Zhao, L., and Huang, W.C. (2012) Element characteristics and prominence analysis of meta-argillo-arenaceous rocks in Zhanggongshan area, Anhui-Jiangxi border region. Geology in China, 39, 1183-1198.

Zhang, Y.X., Liu, Y.M., Gao, S.D., and He, Q.G. (1990) Earth elements geochemical characteristics of tungsten minerals: A distinguishing sign for ore-forming type. Geochemica, 19, 11-20.

Zheng, Y.F., Zhang, S.B., Zhao, Z.F., Wu, Y.B., Li, X.H., Li, Z.X., and Wu, F.Y. (2007) Contrasting zircon Hf and O isotopes in the two episodes of Neoproterozoic granitoids in South China: implications for growth and reworking of continental crust. Lithos, 96, 127-150.

Zhou, X.M., and Li, W.X. (2000) Origin of Late Mesozoic igneous rocks in Southeastern China: implications for lithosphere subduction and underplating of mafic magmas. Tectonophysics, 326, 269 -287.

Zhou, X.M., Sun, T., Shen, W.Z., Shu, L.S., and Niu, Y.L. (2006) Petrogenesis of Mesozoic granitoids and volcanic rocks in South China: A response to tectonic evolution. Episodes, 29, 26-33.

FIGURE CAPTIONS

FIGURE 1. Distribution of the Mesozoic granites and volcanic rocks in South China. Also shown are the location of the Jiangnan orogen and Shimensi ore deposit (modified after Zhou et al. 2006; Deng et al. 2014). The Jiangnan orogen is mainly consisted of greenschist facies Shuangqiaoshan Group meta-sediments (and small amounts of meta-volcanics) with age of 860-825 Ma (detrital zircon ages; Wang et al. 2014) and undeformed Jiuling granite with zircon U-Pb age of 819±9 Ma (Li et al. 2003), which intruded into the Shuangqiaoshan Group.

FIGURE 2. (a) Sketch geological map of the Jiuling Mountains, central Jiangnan orogen, (b) A NE-trending cross-section of the Shimensi deposit showing three ore types: veinlets-type, breccia-type and quartz vein-type mineralization (After No. 916 Geological Team, Jiangxi Bureau of Geology, Mineral Resources, Exploration and Development, 2014), and (c) A NW-trending cross-section showing the major ore bodies in the Shimeisi deposit (After No. 916 Geological Team, Jiangxi Bureau of Geology, Mineral Resources, Exploration and Development, 2014). Also shown are the sampling localities.

FIGURE 3. Veinlets-type mineralization and Breccia-type mineralization
(a) Veinlets-type scheelite hosted in the Neoproterozoic granite from 323m of ZK12008 ; (b) Veinlets-type scheelite hosted in the Neoproterozoic granite under ultraviolet light; (c) Scheelite cross-cut by chalcopyrite in veinlets-type mineralization;

(d) The Neoproterozoic granite and Mesozoic porphyritic granite occurred as fragments welded by ore-bearing quartz; (e) Mineralization in the jigsaw-style hydrothermal breccia; (f) Molybdenite cross-cut by late stage chalcopyrite.

FIGURE 4. Breccia-type mineralization and alteration in the Shimensi deposit (a) Large crystals of wolframite growing inward from the wall towards the vein center; (b) Wolframite-scheelite-chalcopyrite-quartz vein under ultraviolet light; (c) Wolframite cross-cut by late-stage chalcopyrite and pyrite; (d) Raman diagram of fluid inclusions in quartz (see the Fig .3a) coexisting with scheelite from 323m of the ZK12008; (e) Pegmatite shell mainly consisting of K-feldspar, quartz and small amounts of muscovite; (f) Coexistence of scheelite and wolframite in the Mesozoic porphyritic granite. Sch=scheelite, Qtz=quartz, Cpy=chalcopyrite, Wfm=wolframite, Ms=muscovite, Mo=molybdenite, Py=pyrite.

FIGURE 5. Mineral paragenesis for the Shimensi deposit.

FIGURE 6. Plot of MoO_3 vs. WO_3 of scheelites. Scheelite data from other skarn-type tungsten deposits are shown for comparison, including the King Island (Kwark and Tan 1981),the Kara (Zaw and Singoyi 2000) and the Jitoushan and Baizhangyan tungsten deposits (Song et al. 2014).

FIGURE 7. Photomicrographs and cathodoluminescence (CL) images of scheelite in the Shimensi deposit.

(a) Scheelite included in perthite of the porphyritic granite; (b) Intergrowth of scheelite and fluorite in the Neoproterozoic granite;(c) Wolframite and scheelite hosted in quartz vein-type mineralization; (d) The CL image of scheelite hosted in the porphyritic granite; (e) CL images of scheelite hosted in the Neoproterozoic granite; (f) CL image of scheelite hosted in quartz vein. The circle in the CL images of (d), (e), (f) represents analyzed spot by the LA-ICP-MS method, and the numbers beside each circle represent the Eu anomaly values (Table 3). Sch=scheelite, Qtz=quartz, Fl=fluorite, Wfm=wolframite, Per =perthite, Ms=muscovite, Cc=calcite.

FIGURE 8. Chondrite-normalized REE patterns of scheelites from the Shimensi deposit. (a) Scheelites hosted in the porphyritic granite (DHT-138) exhibit complicated REE patterns, with negative Eu anomalies in the scheelites precipitated from "primitive" fluid and positive Eu anomalies in those from more evolved fluid; (b) A single scheelite from the Neoproterozoic granite (DHT-102) exhibit complicated Eu anomalies in the REE patterns, with negative anomalies seen in the center and positive Eu anomalies in the rim; (c) Scheelites in the Neoproterozoic granite (DHT-104) exhibite positive Eu anomalies in the REE patterns; (d) Scheelites hosted in quartz vein show exclusively positive Eu anomalies in the REE patterns; (e) Fluorite coexisted with scheelite hosted in the Neoproterozoic granite shows enriched HREE; (f) Wolframites hosted in quartz vein show no Eu anomalies and enriched HREE in the REE patterns. Scheelites with negative Eu anomalies are shown as red lines, and scheelites with positive Eu anomalies as black lines. Also shown for

comparison are the REE data of the Mesozoic porphyritic granite, fine-grained granites (blue lines; unpublished data), and the granite porphyry (grey lines; unpublished data). The normalization values were from Sun and McDonough (1989).

FIGURE 9. (a) Plot of Na vs. ∑REE+Y-Eu; (b) Plot of Nb vs. ∑REE. Note that all scheelites show REE contents much higher than Na and Nb.

FIGURE 10. (a) Plot of chondrite-normalized Eu concentrations (Eu_N) vs. calculated Eu^*_N values for scheelites, where $Eu^*_N=(Sm_N \times Gd_N)^{1/2}$). Dashed line represents Eu/Eu* = 1; (b) Plot of δEu vs. Na of scheelites; (c) Plot of δEu vs. Mo of scheelites; (d) Plot of δEu vs. Sr of scheelites. See text for explanations.

FIGURE 11. Plots of δEu vs. ∑REE, Sr, and Nb+Ta for scheelites from the porphyritic granite (DHT-138) (a, b, c), and scheelites from the Neoproterozoic granite (DHT-102) (d, e, f). Note that the scheelites with more positive Eu anomalies show lower REE and Nb+Ta and higher Sr abundance.

FIGURE 12. (a) $(^{87}Sr/^{86}Sr)i$ vs. $\varepsilon_{Nd}(t)$ diagram for scheelites of the Shimensi deposit. The Sr and Nd isotopic data of the Mesozoic porphyritic granite, fine-grained granite and granite porphyry are from Mao et al. (2014), the Neoproterozoic granites are from Wu et al. (2006), and the Shuangqiaoshan group rocks are from Zhang et al. (2012). Isotope modeling for a simple mixing between the Mesozoic porphyritic granite and

the Shuangqiaoshan Group, the porphyritic granite with Sr =75.6 ppm, I_{Sr}=0.721, Nd=17.4 ppm, εNd (t) =-5.1; the Shuangqiaoshan Group with Sr =120.6 ppm, I_{Sr}=0.759, Nd=31.1 ppm, εNd (t) =-12.1. (b) Plots of Nb+Ta vs. ($^{87}Sr/^{86}Sr$) for scheelites in the Shimensi deposit. Note that the scheelites precipitated from "primitive" fluid (the porphyritic granites) show higher Nb+Ta and lower Sr isotopic ratios than those from evolved fluids (the Neoproterozoic granites), except one data point with low Sr isotopic ratio, which could be caused by less contribution from the surrounding rocks.

This is a preprint, the final version is subject to change, of the American Mineralogist (MSA)
Cite as Authors (Year) Title. American Mineralogist, in press.
(DOI will not work until issue is live.) DOI: http://dx.doi.org/10.2138/am-2017-5654

TABLES

TABLE 2. Description of the analysed samples

Sample	Number	Description	Location
DHT-91	6	Veinlets-type mineralization in the Neoproterozoic granite	222.7m, Drill ZK11214
DHT-96	10	Veinlets-type mineralization in the Neoproterozoic granite	161.4m, Drill ZK11214
DHT-98	10	Veinlets-type mineralization in the Neoproterozoic granite	162.4m, Drill ZK11214
DHT-102	12	Veinlets-type mineralization in the Neoproterozoic granite	312.4m, Drill ZK11612
DHT-104	10	Veinlets-type mineralization in the Neoproterozoic granite	312.4m, Drill ZK11612'
DHT-131	8	Quartz-vein mineralization	Tunnel PD2
DHT-133	4	Quartz-vein mineralization	Tunnel PD2
DHT-62	11	Veinlets-type mineralization in the Mesozoic porphyritic granite	244m, Drill ZK0408
DHT-138	17	Veinlets-type mineralization in the Mesozoic porphyritic granite	307m, Drill ZK0408

TABLE 4. Rb-Sr and Sm-Nd isotopic data of scheelite samples

Sample no.	Age (Ma)	Sm (ppm)	Nd (ppm)	$^{147}Sm/^{144}Nd$	$^{143}Nd/^{144}Nd$	2σ	$f_{Sm/Nd}$	$^{143}Nd/^{144}Nd(t)$	εNd(t)	$^{87}Sr/^{86}Sr(t)$	2σ

DHT-88	143	--	--	--	--	--	--	--		0.74191	0.0008
DHT-91	143	81.30	277.66	0.1770	0.512206	0.000007	-0.10	0.512040	-8.1	0.75123	0.0007
DHT-92	143	--	--	--	--	--	--	--	--	0.75123	0.0007
DHT-96	143	--	--	--	--	--	--	--	--	0.76153	0.0003
DHT-104	143	11.13	60.58	0.1111	0.512176	0.000002	-0.44	0.512072	-7.5	0.73031	0.0002
DHT-109	143	11.13	60.58	0.1111	0.512187	0.000006	-0.44	0.512083	-7.2	0.76569	0.0003
DHT-124	143	3.63	12.56	0.1747	0.512223	0.000001	-0.11	0.512059	-7.7	0.72353	0.0003
DHT-125	143	3.63	12.56	0.1747	0.512275	0.000007	-0.11	0.512111	-6.7	0.72673	0.0002
DHT-131	143	3.63	12.56	0.1747	0.512239	0.000001	-0.11	0.512076	-7.4	0.72305	0.0004
DHT-145	143	47.74	166.63	0.1732	0.512232	0.000002	-0.12	0.512070	-7.5	0.73674	0.0009
DHT-155	143	2.24	14.38	0.0942	0.512232	0.000003	-0.52	0.512144	-6.1	0.72524	0.0001

Figure 1

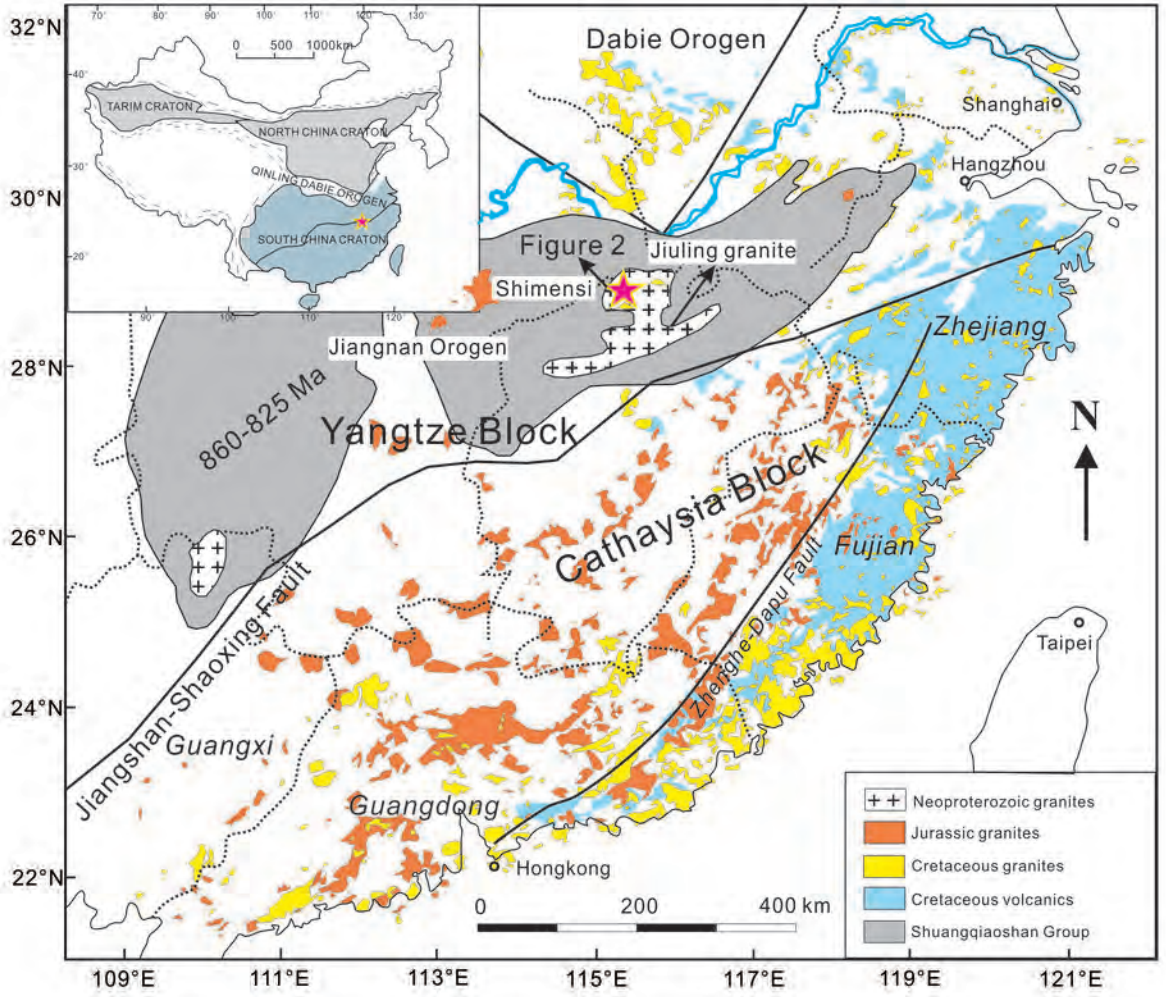
32°N
30°N
28°N
26°N
24°N
22°N
109°E
111°E
113°E
115°E
117°E
119°E
121°E
0 500 1000km
TARIM CRATON
NORTH CHINA CRATON
QINLING DABIE OROGEN
SOUTH CHINA CRATON
Dabie Orogen
Shanghai
Hangzhou
Figure 2
Jiuling granite
Shimensi
Jiangnan Orogen
Zhejiang
860-825 Ma
Yangtze Block
Cathaysia Block
Fujian
N
Jiangshan-Shaoxing Fault
Zhenghe-Dapu Fault
Taipei
Guangxi
Guangdong
Hongkong
0 200 400 km
Neoproterozoic granites
Jurassic granites
Cretaceous granites
Cretaceous volcanics
Shuangqiaoshan Group

Figure 2

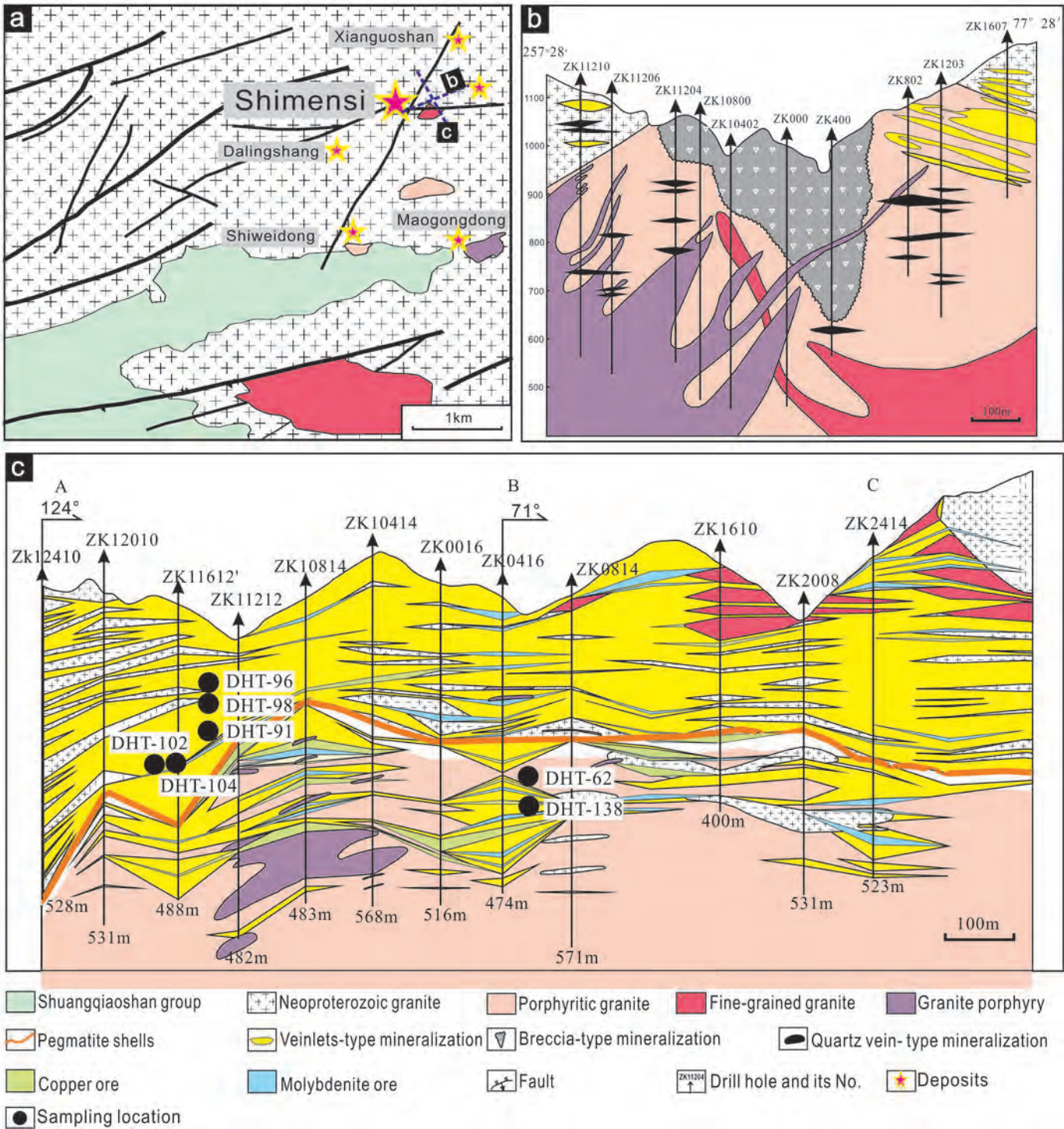
a
Xianguoshan
Shimensi
Dalingshang
Shiweidong
Maogongdong
b
c
1km
b
257°28′
77° 28′
ZK11210
ZK11206
ZK11204
ZK10800
ZK10402
ZK000
ZK400
ZK802
ZK1203
ZK1607
1100
1000
900
800
700
600
500
100m
c
A
124°
B
71°
C
Zk12410
ZK12010
ZK11612'
ZK11212
ZK10814
ZK10414
ZK0016
ZK0416
ZK0814
ZK1610
ZK2008
ZK2414
DHT-96
DHT-98
DHT-91
DHT-102
DHT-104
DHT-62
DHT-138
528m
531m
488m
482m
483m
568m
516m
474m
571m
400m
531m
523m
100m
Shuangqiaoshan group
Neoproterozoic granite
Porphyritic granite
Fine-grained granite
Granite porphyry
Pegmatite shells
Veinlets-type mineralization
Breccia-type mineralization
Quartz vein- type mineralization
Copper ore
Molybdenite ore
Fault
ZK11204
Drill hole and its No.
Deposits
Sampling location

Figure 3

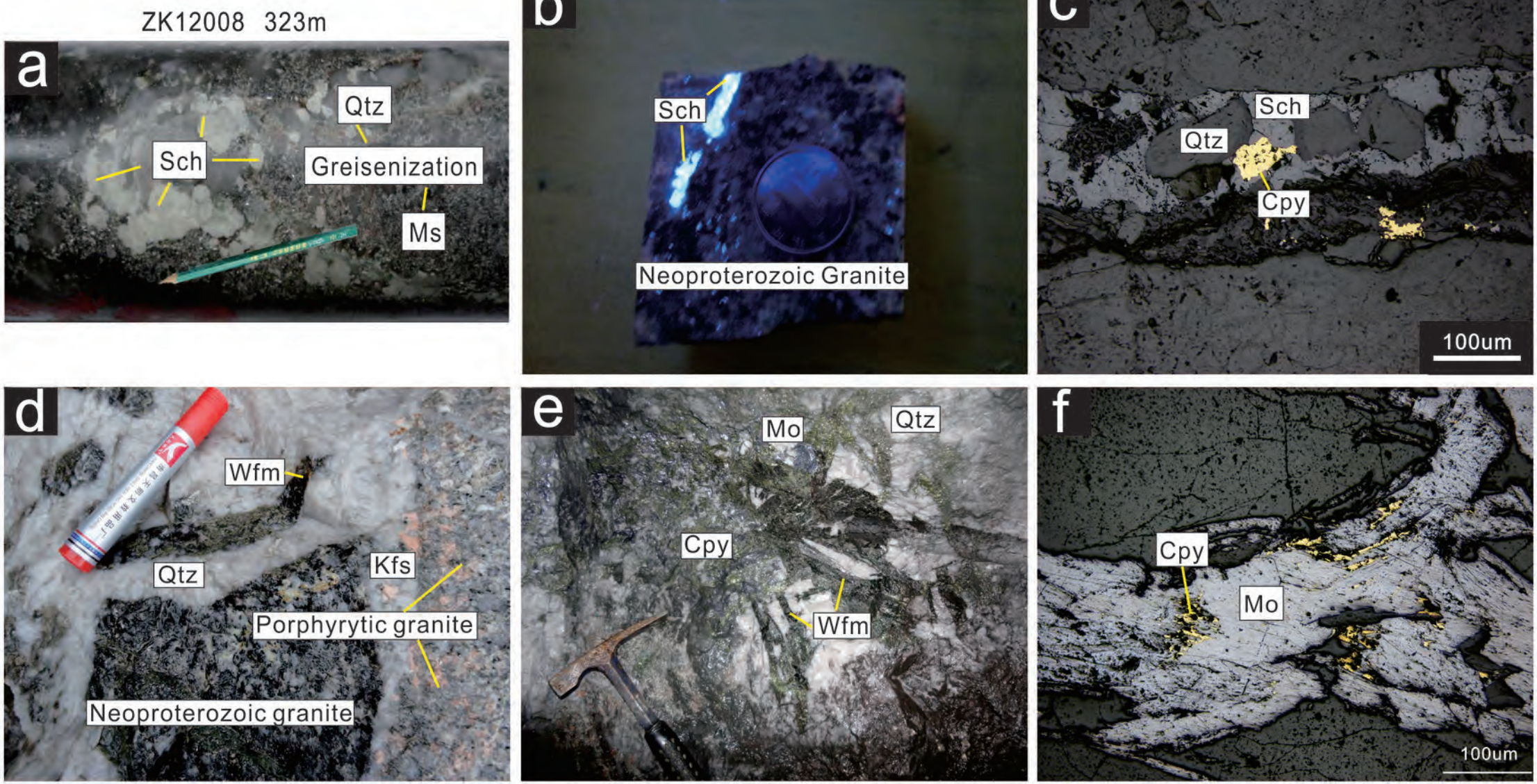
ZK12008 323m
a
Qtz
Sch
Greisenization
Ms
b
Sch
Neoproterozoic Granite
c
Sch
Qtz
Cpy
100um
d
Wfm
Qtz
Kfs
Porphyrytic granite
Neoproterozoic granite
e
Mo
Qtz
Cpy
Wfm
f
Cpy
Mo
100um

Figure 4

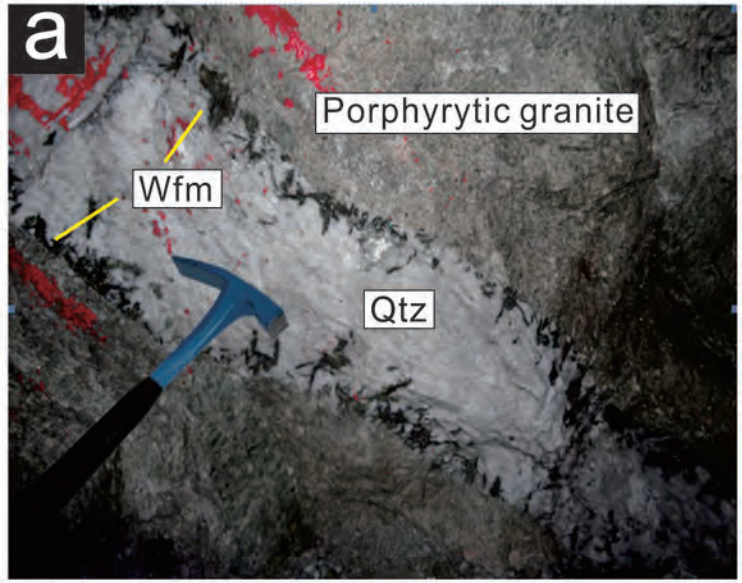
a
Porphyrytic granite
Wfm
Qtz

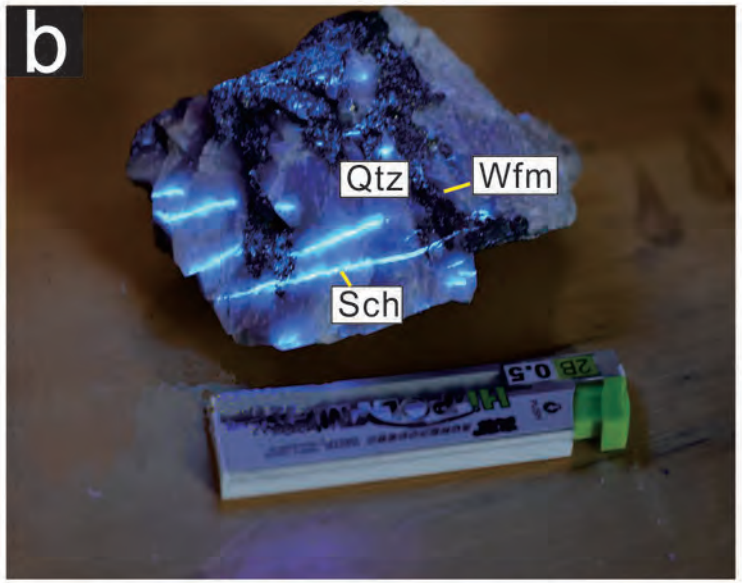
b
Qtz
Wfm
Sch

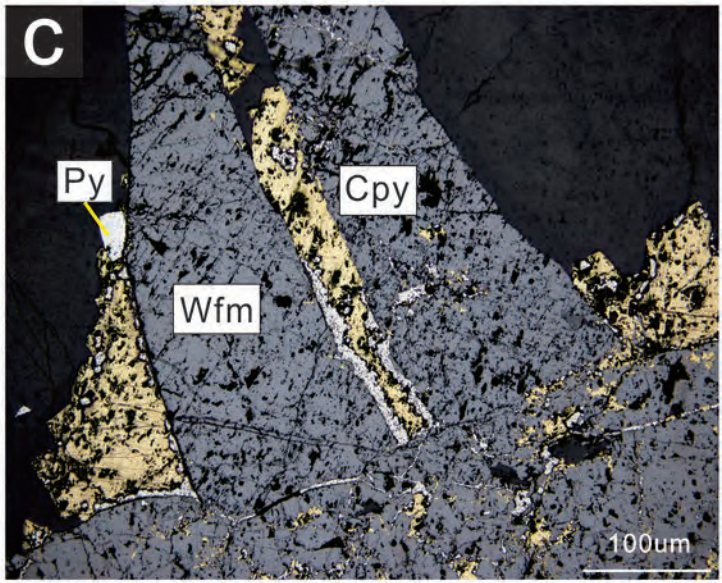
c
Py
Cpy
Wfm
100um

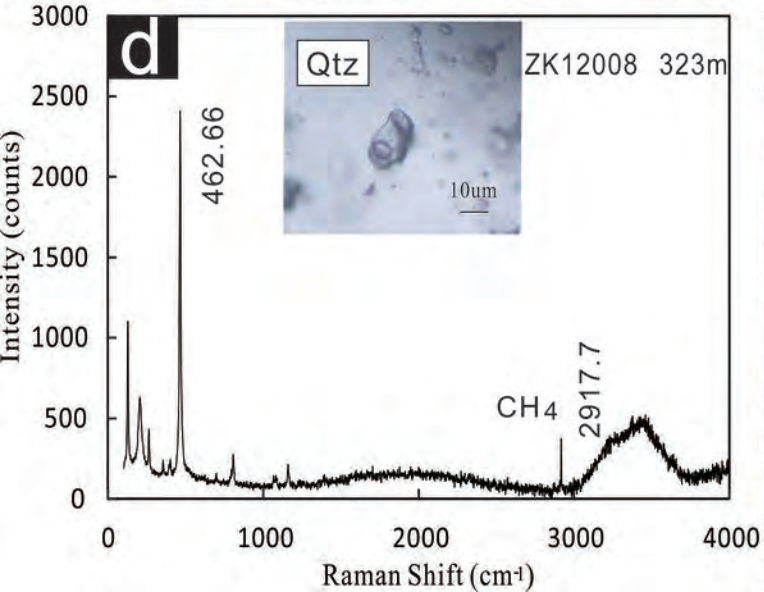
d
Qtz
ZK12008 323m
10um
462.66
CH4
2917.7
Intensity (counts)
Raman Shift (cm-1)
0
500
1000
1500
2000
2500
3000
0
1000
2000
3000
4000

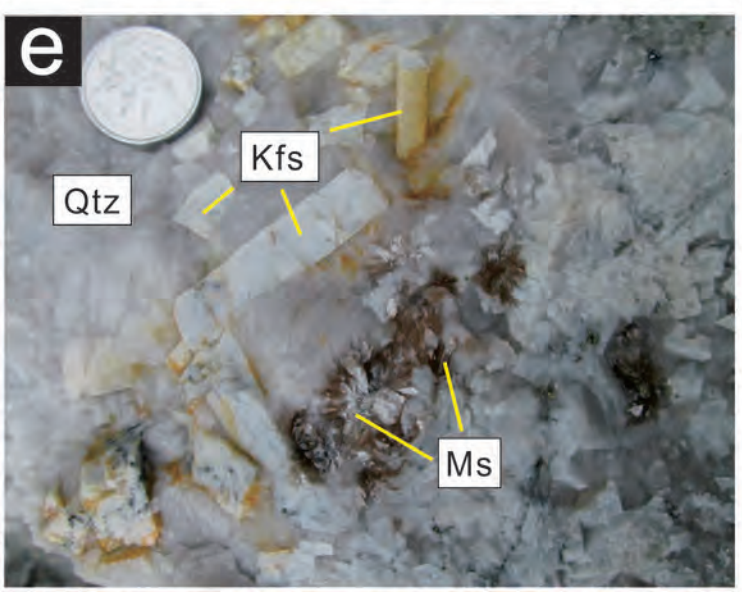
e
Qtz
Kfs
Ms

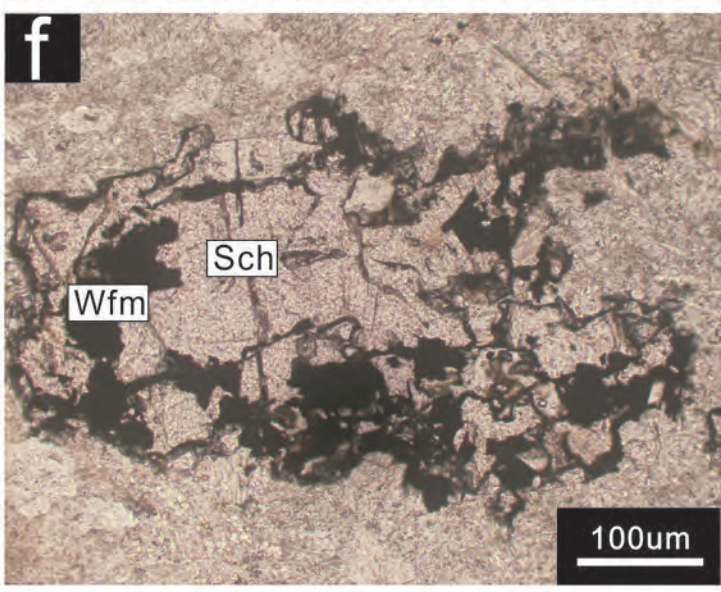
f
Sch
Wfm
100um

Figure 5

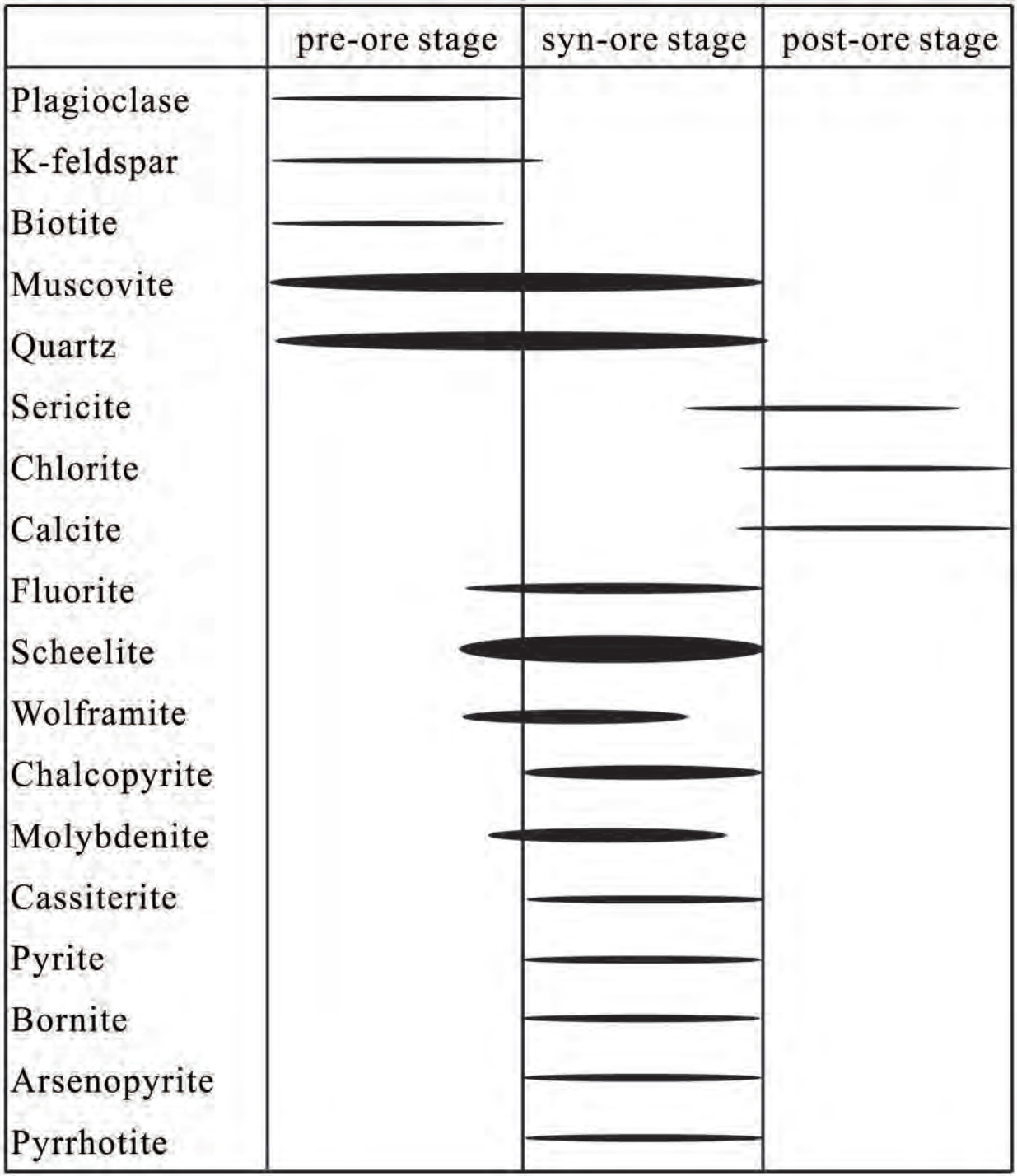
pre-ore stage
syn-ore stage
post-ore stage
Plagioclase
K-feldspar
Biotite
Muscovite
Quartz
Sericite
Chlorite
Calcite
Fluorite
Scheelite
Wolframite
Chalcopyrite
Molybdenite
Cassiterite
Pyrite
Bornite
Arsenopyrite
Pyrrhotite

Fig 6

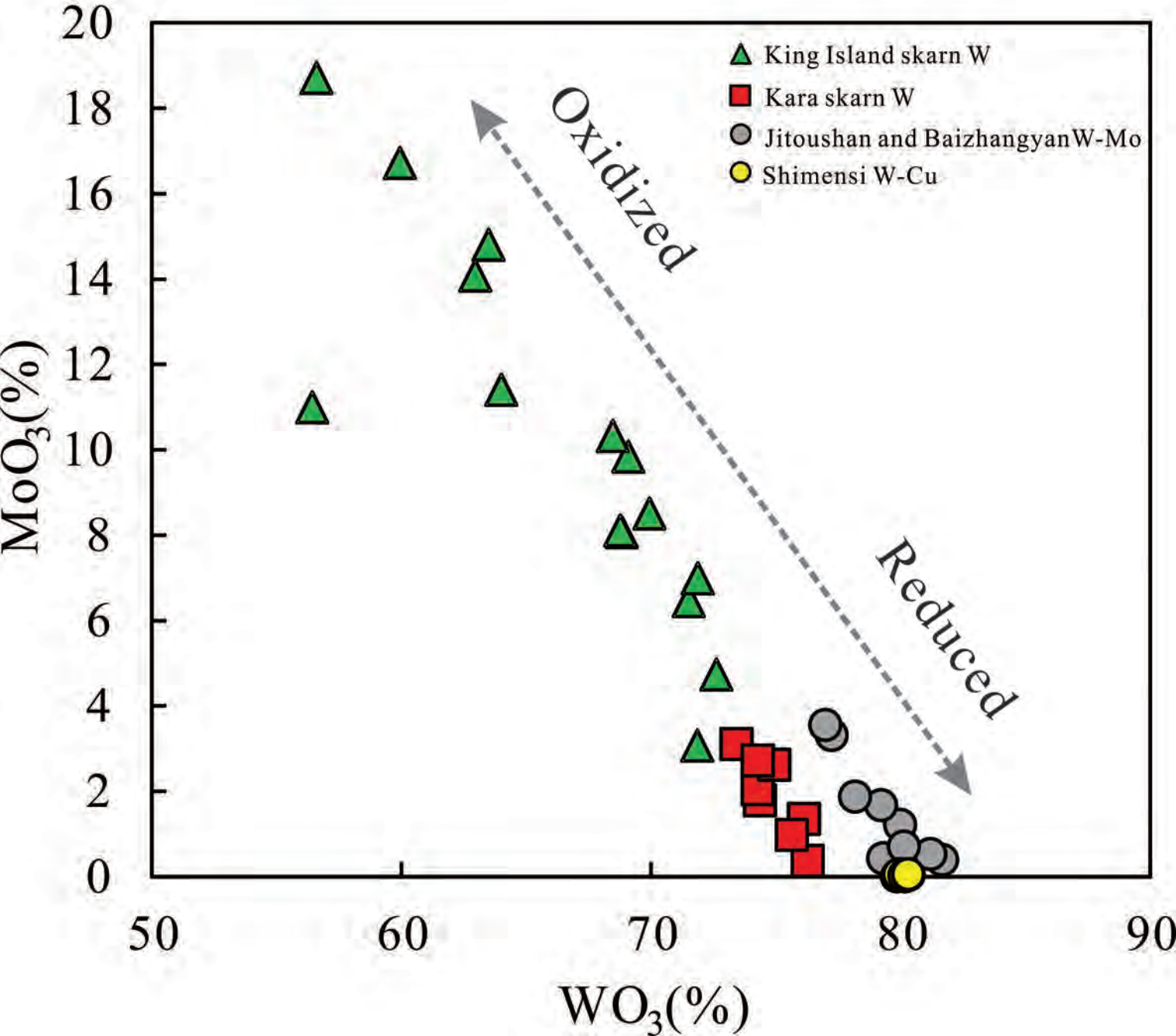
King Island skarn W
Kara skarn W
Jitoushan and BaizhangyanW-Mo
Shimensi W-Cu
Oxidized
Reduced
MoO3(%)
WO3(%)
0
2
4
6
8
10
12
14
16
18
20
50
60
70
80
90

Figure 7

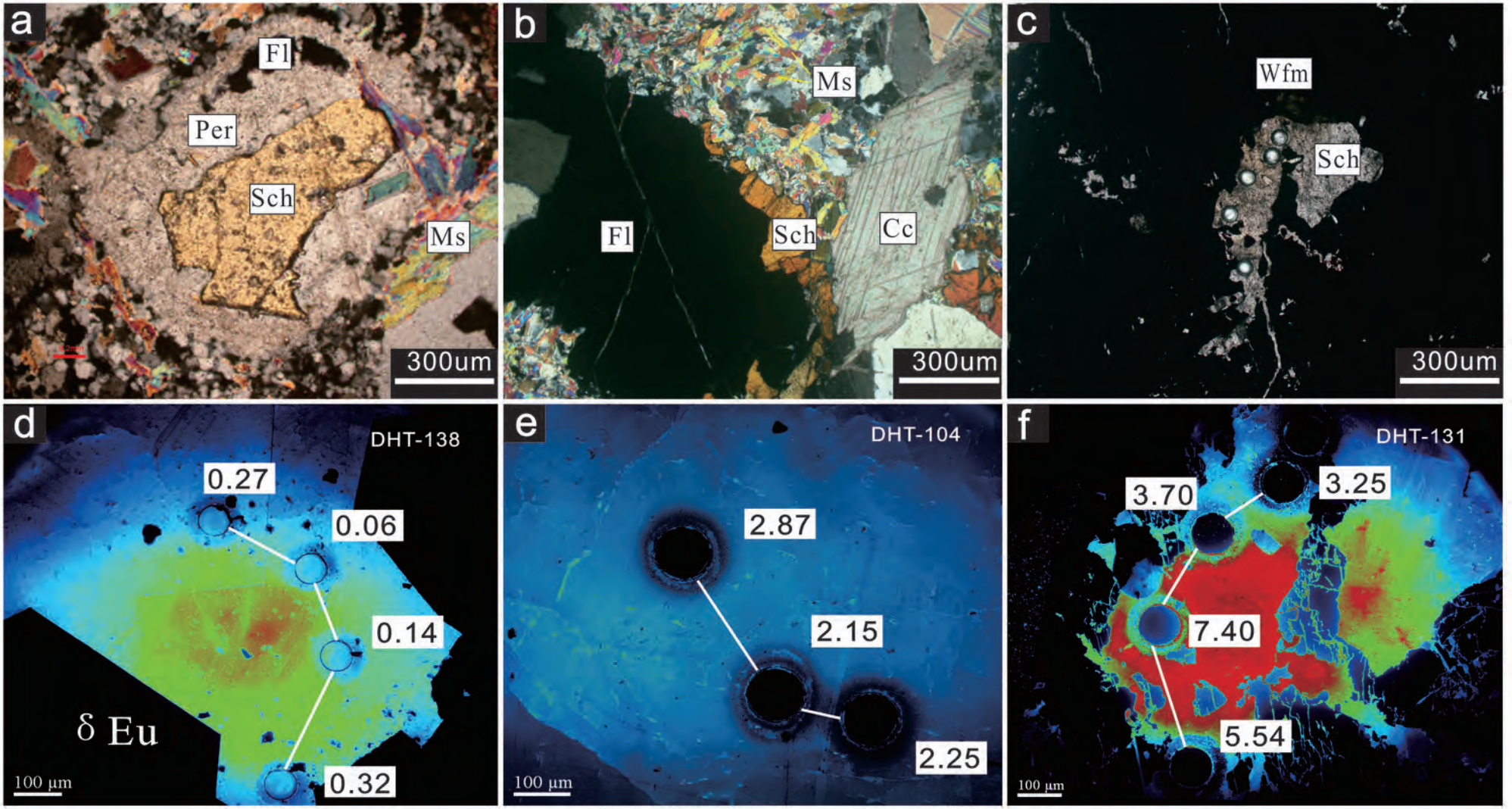
a
Fl
Per
Sch
Ms
300um
b
Ms
Fl
Sch
Cc
300um
c
Wfm
Sch
300um
d
DHT-138
0.27
0.06
0.14
δ Eu
0.32
100 μm
e
DHT-104
2.87
2.15
2.25
100 μm
f
DHT-131
3.70
3.25
7.40
5.54
100 μm

Figure 8

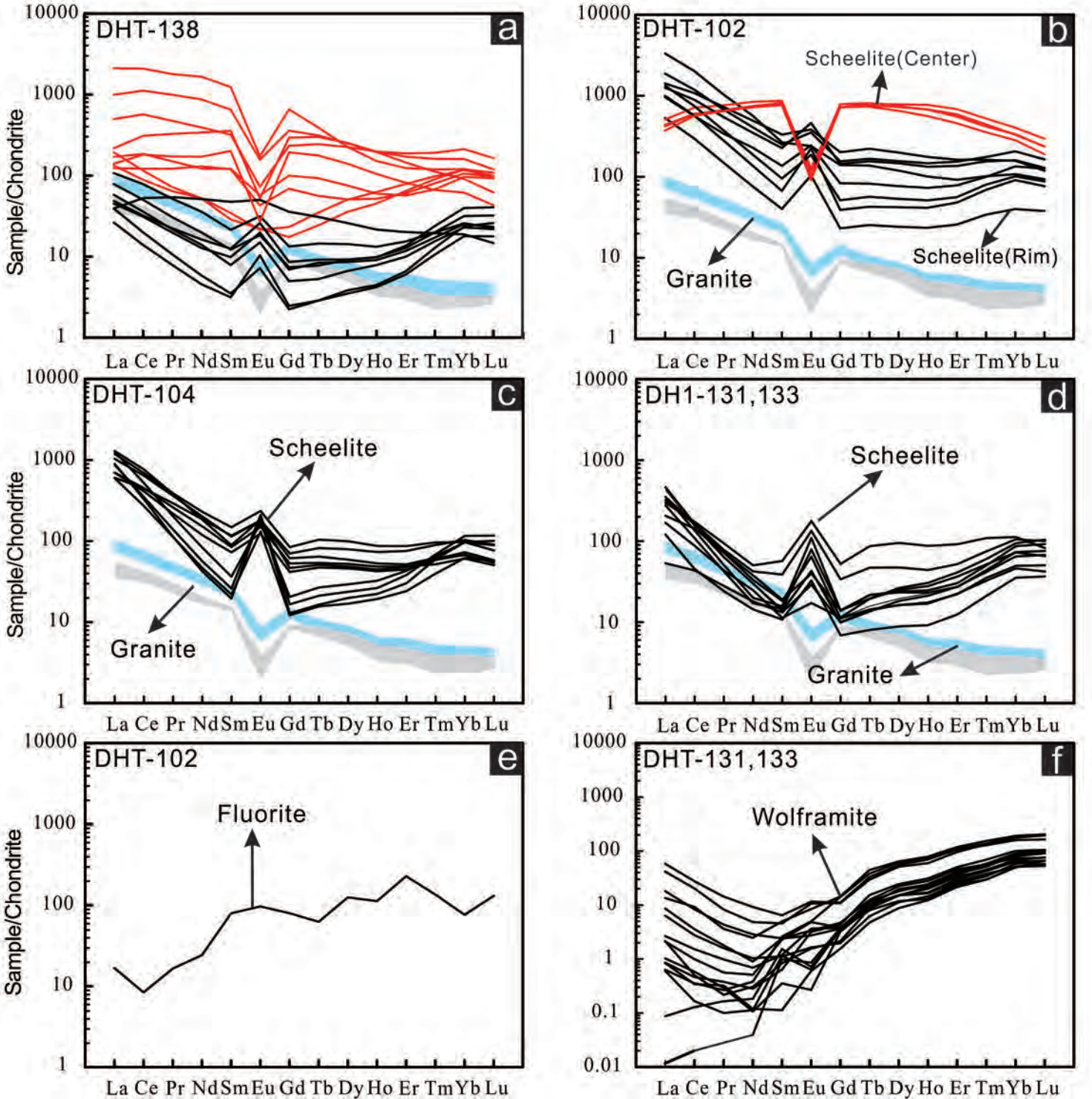
DHT-138
a
Sample/Chondrite
10000
1000
100
10
1
La Ce Pr Nd Sm Eu Gd Tb Dy Ho Er Tm Yb Lu
DHT-102
b
Scheelite(Center)
Granite
Scheelite(Rim)
DHT-104
c
Scheelite
Granite
DH1-131,133
d
Scheelite
Granite
DHT-102
e
Fluorite
DHT-131,133
f
Wolframite
0.1
0.01

Figure 9

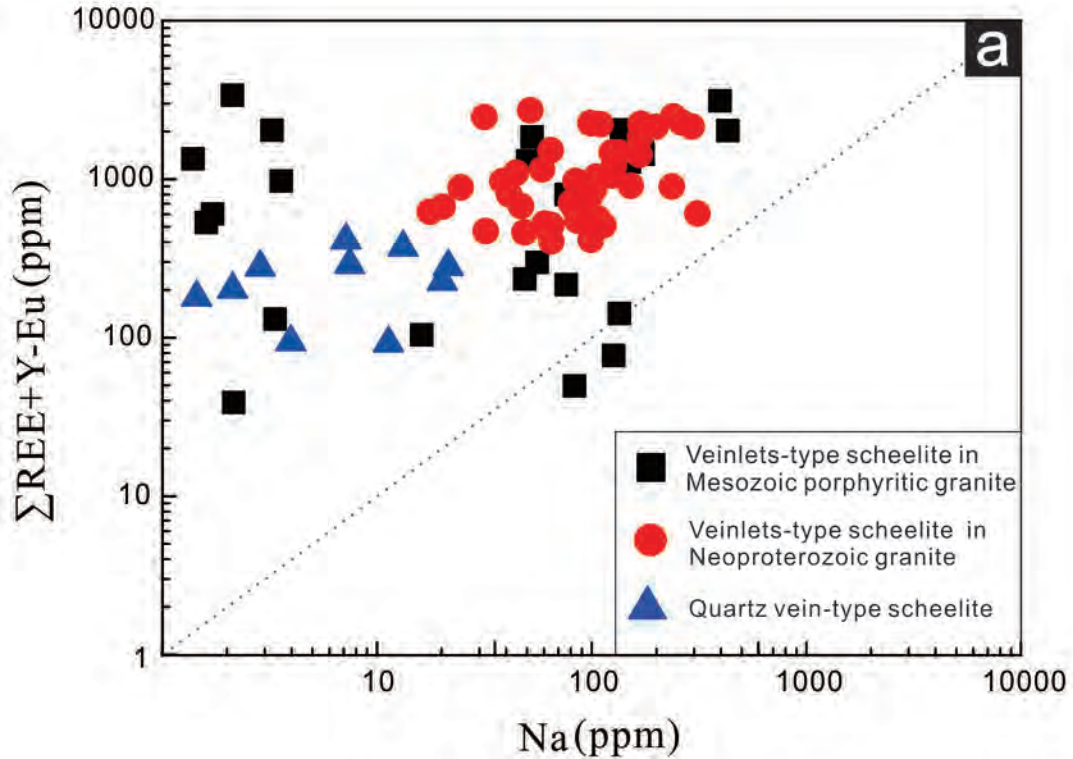
a
10000
1000
100
10
1
10
100
1000
10000
∑REE+Y-Eu (ppm)
Na (ppm)
Veinlets-type scheelite in Mesozoic porphyritic granite
Veinlets-type scheelite in Neoproterozoic granite
Quartz vein-type scheelite

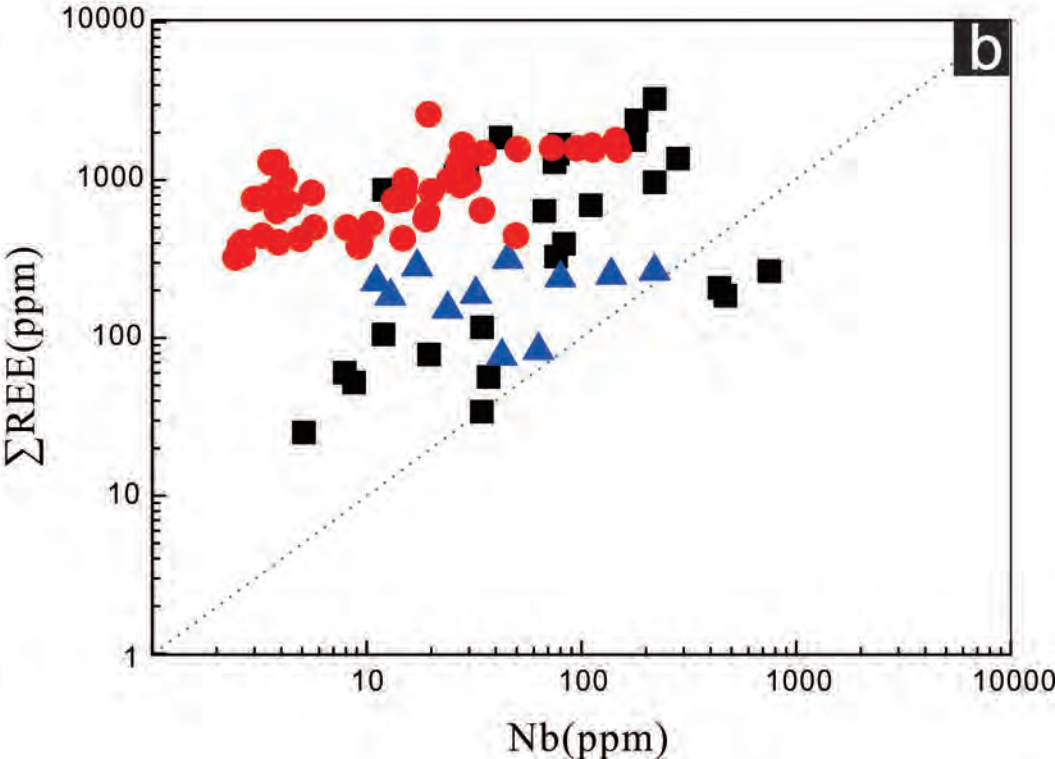
b
10000
1000
100
10
1
10
100
1000
10000
∑REE(ppm)
Nb(ppm)

Figure 10

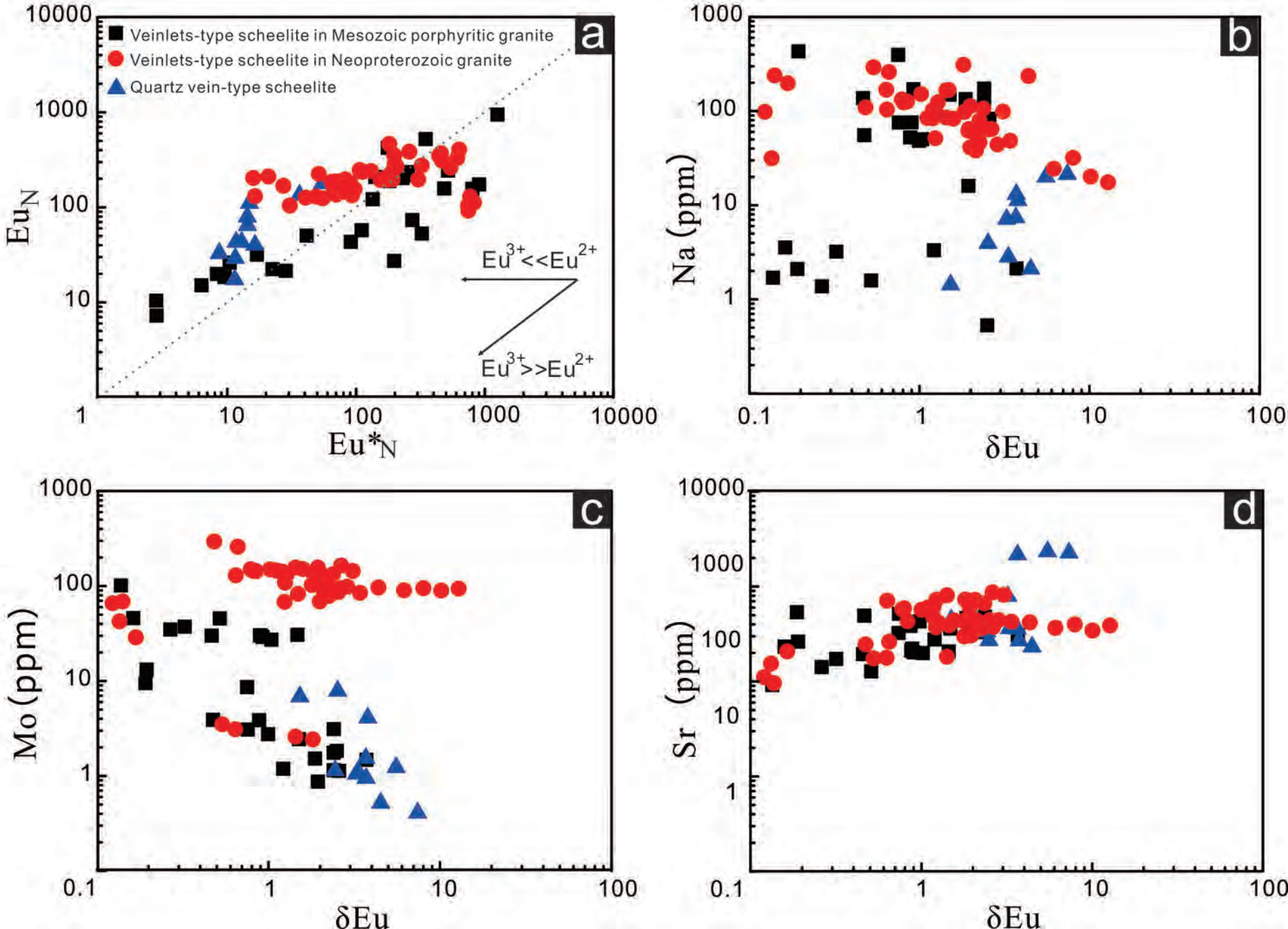
a
Veinlets-type scheelite in Mesozoic porphyritic granite
Veinlets-type scheelite in Neoproterozoic granite
Quartz vein-type scheelite
Eu3+<<Eu2+
Eu3+>>Eu2+
EuN
Eu*N
b
Na (ppm)
δEu
c
Mo (ppm)
δEu
d
Sr (ppm)
δEu

Figure 11

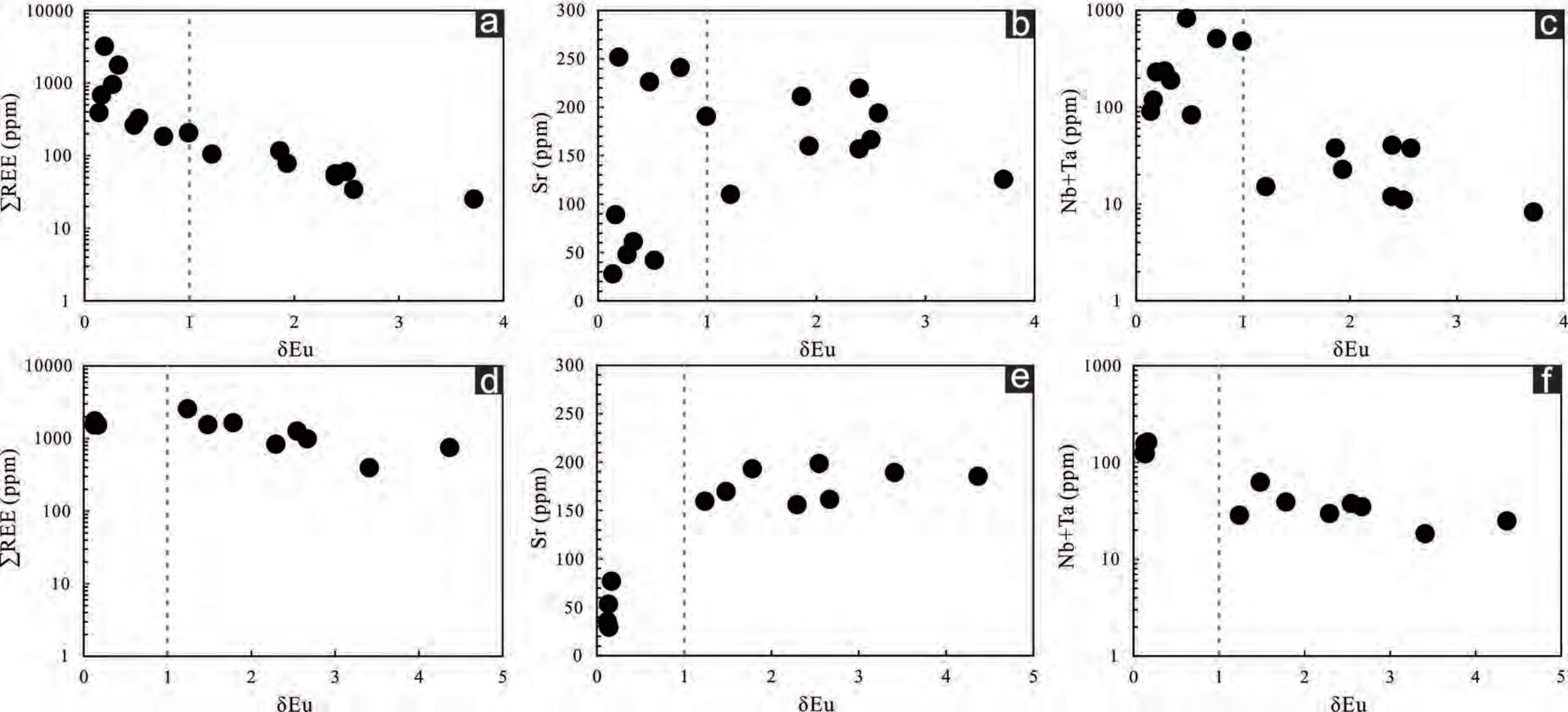
a
b
c
d
e
f
∑REE (ppm)
Sr (ppm)
Nb+Ta (ppm)
δEu
10000
1000
100
10
1
300
250
200
150
50
0
0
1
2
3
4
5

Figure 12

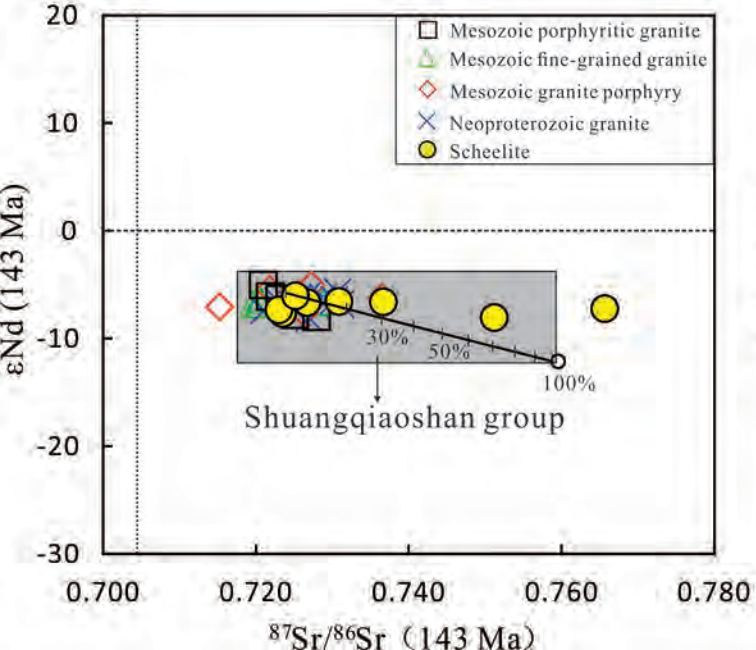
Mesozoic porphyritic granite
Mesozoic fine-grained granite
Mesozoic granite porphyry
Neoproterozoic granite
Scheelite
30%
50%
100%
Shuangqiaoshan group
εNd (143 Ma)
$^{87}Sr/^{86}Sr$ (143 Ma)

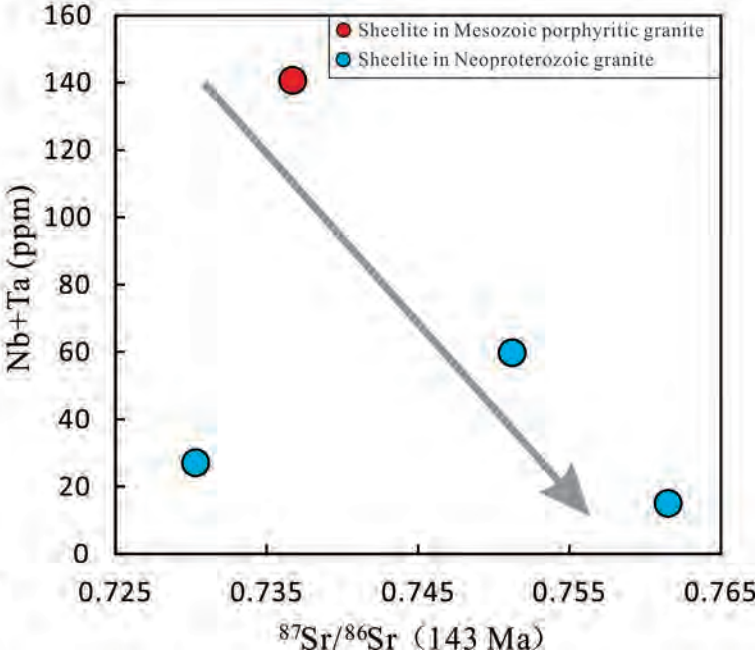
Sheelite in Mesozoic porphyritic granite
Sheelite in Neoproterozoic granite
Nb+Ta (ppm)
$^{87}Sr/^{86}Sr$ (143 Ma)